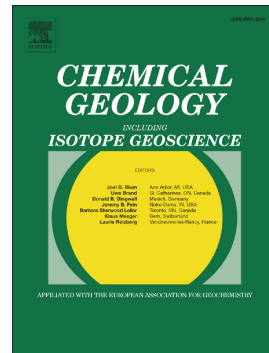


Accepted Manuscript

On the Sr-Nd-Pb-Hf isotope code of enriched, Dupal-type sub-continental lithospheric mantle underneath south-western China

T. Cheng, O. Nebel, P.A. Sossi, J. Wu, W. Siebel, F.K. Chen, Y.J. Nebel-Jacobsen



PII: S0009-2541(18)30238-9

DOI: doi:[10.1016/j.chemgeo.2018.05.018](https://doi.org/10.1016/j.chemgeo.2018.05.018)

Reference: CHEMGE 18771

To appear in: *Chemical Geology*

Received date: 8 January 2016

Revised date: 9 May 2018

Accepted date: 11 May 2018

Please cite this article as: T. Cheng, O. Nebel, P.A. Sossi, J. Wu, W. Siebel, F.K. Chen, Y.J. Nebel-Jacobsen , On the Sr-Nd-Pb-Hf isotope code of enriched, Dupal-type sub-continental lithospheric mantle underneath south-western China. The address for the corresponding author was captured as affiliation for all authors. Please check if appropriate. Chemge(2017), doi:[10.1016/j.chemgeo.2018.05.018](https://doi.org/10.1016/j.chemgeo.2018.05.018)

This is a PDF file of an unedited manuscript that has been accepted for publication. As a service to our customers we are providing this early version of the manuscript. The manuscript will undergo copyediting, typesetting, and review of the resulting proof before it is published in its final form. Please note that during the production process errors may be discovered which could affect the content, and all legal disclaimers that apply to the journal pertain.

**On the Sr-Nd-Pb-Hf isotope code of enriched, Dupal-type sub-continental lithospheric
Mantle underneath south-western China**

T. Cheng^{1,2}, **O. Nebel**^{3*}, P.A. Sossi⁴, J. Wu⁵, , W. Siebel⁶, FK. Chen⁵, Y.J. Nebel-Jacobsen³

¹Beijing SHRIMP Center, Institute of Geology, Chinese Academy of Geological Sciences (CAGS), Haidian District, Beijing, China

²Radiogenic Isotope Facility, School of Earth and Environmental Sciences, The University of Queensland, Brisbane, QLD 4072, Australia

³School of Earth, Atmosphere and Environment, Monash University, 3800 Clayton, VIC, Australia

⁴Institute de Physique du Globe de Paris. France

⁵Chinese Academy of Sciences, Key Laboratory of Crust-Mantle Materials and Environments, School of Earth and Space Sciences, University of Science and Technology of China, 230026 Hefei, China

⁶Department of Geosciences, Tübingen University, Germany

*Corresponding Author: oliver.nebel@monash.edu

Abstract word count: 330

Body Word Count: 6500

No of figures: 11

Abstract

Cenozoic intra-plate volcanism in Southwest China allows insights into modes of melting and the composition of the sub-continental lithospheric mantle (SCLM). The late Cenozoic Tengchong Volcanic Field (TVF), located in the Yunnan Province Northeast of the Himalayas, comprises a cluster of mafic continental intraplate lavas, represented by 68 volcanic cones and spanning an area of ca. 800 km². Major and trace element data and Sr-Nd-Pb-Hf isotope ratios of 18 newly sampled rocks from the area are used to identify the composition of their source in the SCLM. Indices of magmatic differentiation are correlated with isotope composition, marking a classic case of assimilation-fractional-crystallization (AFC) during petrogenesis. The most primitive samples, identified on the basis of element and isotope compositions, are interpreted to be directly derived from the metasomatised mantle underneath south-western China. Modelling of a best-fit scenario indicates that the isotope and trace element character of these samples can be reproduced by ca. 1% partial melting of a metasomatised mantle source, composed of depleted MORB mantle infused with 1% addition of a bulk global subducting sediment (GLOSS) component. Average isotope compositions of $^{87}\text{Sr}/^{86}\text{Sr} = 0.705861$, $^{143}\text{Nd}/^{144}\text{Nd} = 0.512675$, $^{176}\text{Hf}/^{177}\text{Hf} = 0.282962$, $^{206}\text{Pb}/^{204}\text{Pb} = 18.305$, $^{207}\text{Pb}/^{204}\text{Pb} = 15.642$ and $^{208}\text{Pb}/^{204}\text{Pb} = 38.948$ are proposed for the present-day enriched part of the SCLM. The origin of the isotopic signatures is ascribed to modifications of parent-daughter ratios in the SCLM by past subduction-related metasomatism, possibly in the form of sediment mélange diapirs. This implied that the mantle source of TVF lavas is not, as previously proposed, related to enriched geochemical reservoirs (EM-1, EM-2) associated with mantle plume activity or to so-called Dupal or Indian asthenospheric mantle. Instead, it is argued that time-integrated parent-daughter fractionation occurred long before India-Asia

collision and this produced reservoirs with isotopic compositions that resemble some but not all aspects of the Dupal isotope signature. In analogy, so-called Dupal isotope signatures elsewhere may also be the result of contamination of the mantle by a crustal component, most likely subducted sediment.

1. Introduction

The sub-continental lithospheric mantle (SCLM) is the interface between the continental crust and its underlying, convecting, asthenospheric mantle. Its formation is associated with melt extraction from the mantle, leaving a depleted mantle section behind that buoyantly underpins continental crust and is an essential component for craton stabilization (Djomani et al., 2001; Griffin et al., 2003a, 2003b, 2009). Melt-depleted SCLM is commonly re-enriched by fluids and melts through subduction along continental margins (Hawkesworth et al., 1990; Downes et al., 2001; Windley et al., 2010) or alternatively by deeper mantle fluids, for example in relation to eclogitic melting of delaminated crust (Bédard et al., 2006; Wasch et al., 2009; Windley et al., 2010). The complex interplay between depletion and re-enrichment processes and the remote nature of the SCLM make detailed investigations difficult so that composition and age of SCLM remain poorly constrained. Knowledge of SCLM composition is, however, important for constraining formation mechanisms, subsequent evolution through time and for a better understanding of interactions with underlying convecting mantle (Barling et al., 1994; Hoang and Uto, 2003; Rankenburg et al., 2005).

Composition and timing of formation of SCLM can be constrained by studies of xenoliths that are brought to the surface by intra-plate volcanism (Downes et al., 2001; O'Reilly et al., 2001). Isotopic model ages and Re-Os isotope systematics of xenoliths provide the basis for

identifying melt extraction events (Nägler et al., 1997; Reisberg and Lorand, 1995). Subsequent metasomatic enrichment through fluids or melts can be traced using Sr-Nd-Pb-Hf isotopes (Downes et al., 1991; Mukasa et al., 1991; Jiang et al., 2006). Whilst such studies provide important constraints on the processes and timing of melt extraction and re-enrichment, they also highlight the complex chemical and petrological nature of the SCLM. Continental intra-plate volcanism unrelated to mantle plume activity is considered to represent magmatic activity derived directly from the SCLM. Whilst such intra-plate volcanism is usually small in volume and susceptible to assimilation-fractional-crystallisation process (AFC) (e.g., Brandl et al., 2016, Pfaender et al., 2012), defined suites of intraplate lavas with considerable compositional diversity can be used to identify source composition, and possibly processes that led to the formation of lithospheric mantle.

Here we present major and trace element and Sr-Nd-Pb-Hf isotope data for a new set of 18 volcanic rocks from the Cenozoic Tengchong Volcanic Field (TVF) in south-west China (Figure 1). Lithospheric mantle in this area is of considerable interest because of its proximity to the Asia-India collisional orogeny, which has been proposed as an important source for shoshonitic lavas and post-collisional Cu-porphyry deposits (Turner et al., 1996, Hou et al., 2003). The origin of TVF eruptives remains a matter of debate with some arguing for a mantle plume origin, whereas others prefer a derivation from metasomatised lithosphere (see discussion below). In conjunction with published elemental and isotope data from TVF, a model is presented that aims to identify the isotopic code of the SCLM.

2. Geologic background

2.1 Proposed origin of the TVF

Source(s) and related mechanism(s) responsible for volcanism in the TVF area are a matter of ongoing debate. Two opposing hypotheses argue for either: (i) subduction-related magmatism with de-compressional melting of metasomatised mantle sections leading to intraplate volcanism; or (ii) active mantle-plume activity. Zhu et al. (1983) suggested that the majority of lavas is derived from recently metasomatised and heterogeneous mantle in a subduction-collision zone between the Indian and Eurasian plates. Zhao et al. (1992) proposed a new type of post-collisional arc-volcanism along the Myitkyina and Naga Hills suture. In their model they argue for melting of dormant metasomatised sections of the mantle in the aftermath of subduction. Wang et al. (2007) ascribed the volcanic activity to dextral strike-slip motion in the Sagaing area in an intra-continental setting, yet without any influence of active or past subduction.

With reference to intra-plate hot spot volcanism, Cong et al. (1994) and Zhou et al. (1998, 2000) proposed a source component akin to enriched-mantle 2 (EM2), whereas Xu et al. (2012) argued for an enriched-mantle 1 (EM1) composition. Zhou et al. (2012) reviewed earlier work and proposed a hybrid scenario arguing for the subduction of plume-related Ninety East Ridge material and magmatic activity initiated by strike-slip faulting. A two-stage model was proposed by Guo et al. (2015) who argued that magmas were derived from a source produced by metasomatism associated with subduction during the India-Asia collision from 55 to 8 Ma and subsequent melting caused by slab detachment from 8 Ma to the present; this scenario is not dissimilar to the one originally advocated by Zhao et al. (1992).

A major obstacle to deciphering the nature of the Tengchong mantle source is the effect of possible crustal contamination on the compositions of the volcanic rocks; the eruptives are unlikely to represent unmodified primitive magmas. Assimilation fractional crystallization processes can modify elemental and isotope compositions and consideration of these processes has most certainly contributed to the range of models that have been put forward. Difficulties in separating source parameters from contamination mainly relate to unknown degrees of contamination within single lava flows, uncertainty about the chemical nature of the contaminant and the stages of magma evolution at which contamination occurred (Zhou and Jiang, 1998; Ren et al., 2005; Li, 2012; Zhou et al., 2012). Two previous studies argued for strong crustal contamination (Zhu et al., 1983; Mu and Tong, 1987), whereas others (Fan et al., 1999; Chen et al., 2002; Xu et al., 2012) argued that crustal contamination played only a minor role if any. In summary, the mutually exclusive diversity of previous hypotheses and the lack of a unified model that integrates all geochemical observations stems from: (i) the complicated tectonic regime of south-western China with a long history of subduction, amalgamation and crustal reworking; and (ii) the selection of rock types or study areas, which may not allow a comprehensive assessment of the liquid line of descent or a quantitative assessment of the potential effects of AFC. In this study, all major rock types and areas are sampled and compared with existing data in order to present a coherent model that enables the effects of AFC to be evaluated and the compositions and origins of mantle sources to be constrained.

2.2 Geologic setting and sample description

The Tengchong block is situated in the western Yunnan Province in the south-west of the People's Republic of China near the border with Myanmar. It lies to the East of the Himalayas, within the suture zone system between the Indian and Eurasian plates with several major faults and fold belts. The block is part of the Tibet-Yunnan Fold System, which belongs to the south-eastern margin of the Tibetan Plateau. Within the Tengchong block, from west to east, important fault and suture zones are the Naga Hills paleo-subduction zone, the Sagaing dextral fault, and the Myitkyina-Mandalay suture zone. To the East of the Tengchong block, the high-grade Gaoligong metamorphic belt is intruded by numerous I-type granites, ranging in age from Late Mesozoic to early Cenozoic (Figure 1). These 68-53 Ma granites are thought to be the continuation of the Gangdese magmatic granitoid batholiths, which are considered to be related to the subduction of Neo-Tethyan Oceanic lithosphere (Zhou et al., 2012).

The greater study area in the TVF comprises a series of Cenozoic intraplate volcanic centers and shallow intrusions. The TVF is exposed over most of the Tengchong block, is of late Miocene to Quaternary age and was emplaced in a large basin structure. It covers an area of ca. 800 km², and consists of about 68 volcanoes of various sizes, mainly along the Gaoligong dextral strike-slip fault. Based on early studies, volcanism started at ~5.5 Ma (Zhu et al., 1983; Mu and Tong, 1987; Li et al., 2000; Yin and Li, 2000; Wang et al., 2006), whereas more recent whole-rock Ar-Ar age determinations suggest an age range from 8 Ma to historic eruptions (Guo et al., 2015). The volcanic eruptions from the Miocene over the entire Quaternary period can be divided into four stages: (1) late Miocene to early Pliocene, mainly with olivine-phyric basalt; (2) early Pleistocene andesite, olivine basalt and dacitic tuff; (3) late Pleistocene olivine basalt and andesitic basalt; (4) Holocene olivine basalt and basaltic andesite (Fan et al., 1999,

2001; Li et al., 2012). Volcanic eruption centres migrated with time from the eastern and western margins towards the centre of the basin (Zhao and Chen, 1992; Jiang, 1998, Guo et al. 2015).

A total of eighteen locations along the major strike-slip trends were sampled, with five central basin, eight western margin, two eastern margin and three southern margin samples. According to the current understanding of the temporal evolution of the basin, the samples were subdivided into ten samples from the older, outer eastern and western part of the volcanic field, (Unit 1, olivine-bearing alkaline basalt; Neogene, Figure 1), and five samples from the younger, central eruptions (Unit 2, alkaline basalt without olivine; Quaternary, Figure 1). The three southern samples from the border of the Tengchong and Luxi blocks along the Ruili-Mandalay Fault have a more acidic character. These are therefore grouped as a separate chemical-spatial unit (Unit 3). Sample (13LX02) is a carbonate country rock and was collected with the intention of using the sample as a possible country rock contaminant endmember.

3. Analytical methods

For each sample, ca. 2 kg of rock was collected from surface exposed outcrops. Fresh rock material, free of weathered rims, was crushed at Langfang Laboratory of Geophysical Exploration, Hebei, China, and powdered in an agate mortar. Major element oxides and minor elements were analyzed at James Cook University in Townsville, Australia, using X-ray fluorescence (XRF) and fused lithium-tetraborate discs and a Bruker-AXS S4 Pioneer X-ray Fluorescence Spectrometer. Trace element compositions (except for the carbonate 13LX02) were determined by laser-ablation inductively coupled plasma mass spectrometry (LA-ICP-

MS) at the Australian National University (ANU) using the same fusion discs that were used for XRF analyses. For this, Si was used as an internal standard element, NIST-610 glass as standard reference material with reference values for trace elements listed in of Jochum et al. (2011). BHVO-2 glass as an internal standard to test data reproducibility. Analytical precision of major and trace elements is typically better than 5%. Major and trace elements are listed in Tables 1 and 2.

The Sr-Nd-Pb isotopic ratios were measured on a Finnigan MAT-262 mass spectrometer at the University of Science and Technology of China following the procedure given in Chen et al. (2002). Prior to isotope analyses, ca. 100 mg of rock powder was dissolved in an acid mixture of HNO₃-HF in 15 ml Savillex vials on a hotplate. After successful dissolution, all samples were treated three times with concentrated nitric acid to break possible CaF bonds. Purification of Sr-Pb was performed using Eichrom Sr resin™ and different molarities of HNO₃ following the procedure outlined in Pin et al., (2014). Neodymium was separated from the sample matrix using Eichrom TRU and Ln resins that are described in detail in Pin et al., (2014), yet without the described tandem-column chemistry. Both, Sr and Nd isotopic compositions were corrected for instrumental mass fractionation using values of ⁸⁶Sr/⁸⁸Sr=0.1194 and ¹⁴⁶Nd/¹⁴⁴Nd=0.7219, respectively. The Pb isotopic ratios were corrected for thermal fractionation of 0.11% per atomic mass unit based on the repeated analyses of the NBS-981 standard. Hafnium was purified from a separate batch of powder with a similar volume and dissolution technique compared to the Sr-Nd-Pb procedure. The purification followed the protocol of Cheng et al. (2014) that allows the collection of Fe for stable isotope analyses, which will be subject to a subsequent study. Hafnium isotopes were determined using a Thermo Fisher Neptune *plus* multi-collector inductively coupled plasma mass

spectrometer housed at the ANU and followed procedures outlined in detail in Nebel et al. (2009). In brief, measured $^{176}\text{Hf}/^{177}\text{Hf}$ were mass bias corrected using a $^{179}\text{Hf}/^{177}\text{Hf}=0.7325$. The reported $^{176}\text{Hf}/^{177}\text{Hf}$ were further corrected to a JMC-475 standard value of $^{176}\text{Hf}/^{177}\text{Hf}=0.282160$ for instrumental drift for the analytical session. Using the above outlined procedures, the blanks for all isotope systems were Sr = 30 pg, Nd= 100 pg, Pb=100 pg, and Hf=15 pg and thus negligible (all isotope data are shown in Table 3).

Geochemical modelling of the evolution of the Tengchong volcanic rocks was performed assuming a spinel peridotite bulk composition, with mineral proportions and bulk composition equivalent to DMM (depleted MORB mantle) using values of Workmann and Hart (2005). A description and modelling parameters are given in the appendix. Olivine and orthopyroxene partition coefficients were compiled from the GERM database (<http://earthref.org/>), whereas those of clinopyroxene are from Hart and Dunn (1993). Mathematical expressions for the partitioning of trace elements between liquid and residue according to mass balance and equilibrium between the two phases (batch melting) are used (Shaw et al., 1970). Purely modal melting was modelled and the addition of bulk endmembers was assumed. These endmembers are upper - , lower continental crust (both after Rudnick and Gao 2003) and global subducting sediment (GLOSS, after Plank & Langmuir, 1998). Bulk subducting sediment addition rather than partial melts thereof are considered feasible here as to the addition of sediment melanges to the sub-arc mantle (Marschall and Schumacher 2012).

4. Results

4.1 Major and trace elements

Seventeen volcanic samples and one coarse grained plutonic rock analysed in this study (Table 1A lists locations of the samples) cover a wide range in major element composition. In

a total alkali vs. silica diagram (TAS, Figure 2), compositions vary from basaltic to rhyolitic. Whilst most samples cover basaltic to trachy-andesitic compositions, one sample plots in the dacite field and two samples are rhyolitic in composition. The latter three samples (Unit 3) are differentiated on the basis of their extreme degrees of fractionation and their spatially distinct location (section 2.1). In comparison with published data for the TVF, our samples cover the entire spectrum of reported analyses. In general, samples from Unit 1 are more mafic than those of Unit 2. Sample 13LX10 is a coarser grained igneous rock, which falls outside the IUGS classification for plutonic rocks, but plots close to gabbro (not illustrated).

In major element diagrams (Figure 3), all samples show trends consistent with typical crystal fractionation of evolving basaltic liquids. The most Mg-rich samples overlap in composition with global MORB and follow a trend towards higher SiO₂ with decreasing MgO content. The TVF rocks are low in CaO for a given K₂O content, which reflects their alkaline character. In a TiO₂ vs MgO plot (Figure 3), the rock suite lies on a shallower sloping trend compared to that defined by evolving MORB, with preferential removal of Ti in the TVF liquids before a break in slope at ca. 4 wt. MgO, which most likely marks the onset of magnetite saturation (cf. Jenner et al., 2010).

The trace elements of the volcanic rocks show a considerable spread in absolute concentrations, as shown in Figure 4 in a chondrite-normalized multi-element diagram. All samples are enriched relative to primitive mantle by 10 to 100 times. Some samples exhibit pronounced positive Th-U, Pb and Zr-Hf anomalies combined with Sr, Nb-Ta and Ti depletions. When the abundances of Nb, as a highly incompatible element, and Ni, which is compatible in olivine, are plotted against MgO content and compared to MORB (Figure 5), it becomes clear that the volcanic rocks are relatively enriched in high-field-strength elements (HFSE), but

have Ni concentrations similar to those of MORB. The rare earth elements (REE) are also enriched by >100 times chondritic abundances for the light REE (Figure 4, small inlet) with a slight negative slope in the heavy REE. Most volcanic rocks exhibit a negative Eu/Eu* (i.e., Eu/[(Gd+Sm)/2]) anomaly with the notable exception of the Unit 3 rhyolitic rocks (13LX01, 13LX03, 13LX04). The plutonic sample shows complementary trace element patterns when compared to the volcanic rocks with, for example, a positive Eu/Eu* anomaly.

4.2 Isotope results

The Sr-Nd-Pb-Hf isotope composition of the 18 igneous rocks is distinct from that of the depleted mantle and spans over a wide range (Table 2). The three high Si rocks of Unit 3 (13LX01, 13LX03, 13LX04) are the most isotopically evolved samples and show a strong affinity towards local upper crust composition (Figures 6,7). The other 15 volcanic rocks have a more limited range in Sr-Nd isotopes but, nonetheless, $^{87}\text{Sr}/^{86}\text{Sr}$ ratios range from 0.7057 to 0.7089, and ϵ_{Nd} values from -5.6 to +0.9. The $^{206}\text{Pb}/^{204}\text{Pb}$ ratios range from 18.07 to 18.32, with $^{207}\text{Pb}/^{204}\text{Pb}$ from 15.64 to 15.69, and $^{208}\text{Pb}/^{204}\text{Pb}$ from 38.94 to 39.19. All Pb isotopic compositions plot above the northern hemisphere reference line (NHRL, Hart et al., 1984, Figure 7), yet Pb isotopic compositions are seemingly distinct from the Indian or Dupal mantle field (e.g., Pearce et al., 2007, Dupres and Allegre 1982), represented here by data from the Central Indian ridge (Figure 7). The $^{176}\text{Hf}/^{177}\text{Hf}$ of the volcanic rocks show a distinctively larger range in isotope composition when compared to Nd, with a range from 0.282586 to 0.282986, corresponding to ϵ_{Hf} values of -6.6 to +7.6. The combined Nd-Hf isotope data for the Tengchong volcanic rocks are broadly correlated, yet show an offset from the terrestrial array (Vervoort and Blachert-Toft, 1999) in a curvilinear trajectory, and a clear trend from primitive mantle compositions towards more evolved, crust-like compositions (Figure 6). Sample 13LX-

10 shows a strong deviation from the cluster of mafic volcanics with an isotopic composition trending towards that of local crust.

In comparison with previously published isotope compositions for the TVF, our data fall within the range of reported values (Zhu et al., 1983; Chen et al., 2002; Zhou et al., 2012; Dapeng et al., 2012; Li et al., 2012). Notable is that literature values for Eastern China are more primitive in isotope composition (Zou et al., 2000). However, these plot on distinctively different trends and seemingly represent MORB mantle derivatives and thus not enriched mantle. In the Yunnan Province of Eastern China, and in the TVF in particular, there are no reported radiogenic isotope literature values that are more primitive than our most primitive samples. Hence, it appears that the intraplate lavas of south-western China are sourced from isotopically distinct mantle.

5. Discussion

5.1 Identification of source mineralogy and metasomatism

Identification of the source mineralogy of melts, and thereby their source chemistry, is not straightforward. Controlling factors for the chemical composition of primary melts are the degree and depth of melting, and source composition. In a primitive mantle normalized trace element diagram, the TVF rocks are characterized by enrichment of LILE (large ion lithophile elements) and LREE with negative Nb-Ta-Ti anomalies and elevated Pb abundances (Figure 4). This pattern is traditionally explained by subduction-induced metasomatism, i.e., mantle modified by slab-related fluids and/or subducted sediment melts (Alabaster et al., 1982; Pearce and Parkinson et al., 1993; Marschall and Schumacher et al., 2012). This is consistent with the scenario proposed by Guo et al. (2015), that subduction-derived fluids have affected

the Tengchong eruptives' mantle source. Combined with elevated K₂O abundances, it seems plausible to assume that a source that produces such distinct element patterns is likely to have contained phlogopite/phengite (\pm amphibole). These minerals can form by reactions of slab-derived agents with ambient mantle (Pirard and Hermann, 2015; Spandler and Pirard, 2013), and are not uncommon phases in mantle xenoliths derived from the SCLM (Witt-Eickschen et al., 2007). There is a line of argument that support this hypothesis. The partial breakdown of these hydrous phases would allow partial melting through the release of volatiles, which carry a LILE signature. Depletion in Nb-Ta and Ti is further expected by means of retention of these elements in rutile, unless they melted out completely, which is not expected for low degree lithospheric melts (e.g., Aulbach et al., 2008). Indeed, similar element systematics have been observed in shoshonitic rocks from the Himalaya and have been interpreted to indicate melting of metasomatised mantle (Turner et al., 1996, Hou et al., 2003).

Although the TVF lavas are depleted in Nb-Ta compared to other elements of similar compatibility, it is clear that overall the absolute HFSE abundances are systematically enriched in these rocks relative to MORB. If this enrichment is to be explained by crustal contamination, then the level of crustal input is greater than would be expected, based on radiogenic isotope compositions. These indicate only small amounts of crustal involvement. Based on the rationale outline above, a working hypothesis has been developed in which the source of the TVF lavas is assumed to have a mineral assemblage modified by metasomatism, as is commonly demonstrated to be the case in SCLM (e.g., Griffin et al., 2003a). The major element compositions of the most primitive TVF samples indicate that they have been affected by only minor crystal fractionation so that partial melting calculations and modelling of trace element

patterns may constrain the origin of the observed trace element and isotopic signatures. It is important to stress, however, that the majority of the samples studied here have evidently undergone various degrees of post-melting modification and this precludes a straightforward assessment of the composition of the mantle source.

5.2 Assimilation vs. fractional crystallization

Based on petrographic and major element patterns, the plutonic sample 13LX10 is classified here as a cumulate rock, with accumulated clinopyroxene plus feldspar, which is also indicated by enrichment of CaO and MgO relative to the basalts. This cumulus nature is apparent in the chondrite-normalized REE pattern; with a positive Eu/Eu*, whereas most other rocks have slightly negative Eu anomalies consistent with feldspar removal. The same can be observed in the primitive-mantle normalized multi element plot with complementary negative and positive Sr spikes in the volcanic rocks and the cumulate, respectively (Figure 5). This sample can thus be excluded from further discussion, but serves as a measure for cumulate behaviour, evidence for which is not observed in any other rocks.

The behaviour of the major elements, (Figure 3) in the lava suite of the TVF is consistent with crystal fractionation controlled by the removal of olivine, clinopyroxene and feldspar. It is, however, notable that the major element trends deviate from those that characterize MORB fractionation. CaO and TiO₂ abundances are lower in the TVF lavas and this is likely to be related to differences in source mineralogy, or pressures and degrees of melting. If the spatial distinctions defined for the units (section 2.1) are considered, more striking compositional difference become obvious with Unit 1 containing more primitive lavas and Unit 2 distinctively more evolved ones. These petrological distinctions are reflected in an age

progression from the central (Unit 1) to marginal (Unit 2) parts of the TVF, suggesting the tectonic setting played a role in governing the chemistry of the erupted lavas. The distinction between units is further reflected in a slightly more alkaline character in unit 1.

Whilst major element systematics are consistent with control by fractionation crystallization, radiogenic isotopes are not affected by this process. However, the radiogenic isotopic compositions of Unit 2 samples also change with the degree of differentiation, so for these samples, magmatic evolution cannot have taken place in a closed system; some degree of crustal assimilation is necessary. Assimilation with crystal fractionation is illustrated in a diagram of ε_{Nd} vs. MgO abundance (Figure 8) with a clear trend of decreasing isotopic ratio with decreasing MgO content. Group 1 samples are only slightly affected, if at all. It appears that most rocks have undergone various levels of crustal assimilation during crystal fractionation.

Given the significance of AFC processes involved in generating the lavas, insight into the nature of the mantle source is best constrained by taking the least evolved samples, identified by the least evolved Nd, Hf and Sr isotope compositions. Three samples (13LX09, 13LX11, 13LX12 from Unit 1) have relatively similar isotope compositions with $\varepsilon_{\text{Nd}} \sim +1$, $\varepsilon_{\text{Hf}} \sim +7$ and $^{87}\text{Sr}/^{86}\text{Sr} \sim 0.706$ and are among the most primitive lavas reported in the Tengchong area. With relatively high Mg# (64), two of these have presumably been modified by only minor fractional crystallization of olivine.

5.3 Modelling of melting and source characteristics

A test for the feasibility of the primitive nature of samples 13LX09 and 13LX11 is a comparison of partial melting and crustal assimilation models. Isotopically, these most

primitive samples have $\varepsilon_{\text{Nd}} \sim +1$. Although this is mantle-like, it still indicates the presence of a crustal component. Elemental ratios indicative of crustal influence, such as elevated Th/U or lower Nb/U compared to mantle rocks, support this. Combined, these proxies suggest that these melts have either been affected by minor crustal contamination and are not directly derived from the mantle source, or that they are derived from a source that itself has been modified prior to melting, e.g., through metasomatism. To distinguish between these two scenarios, we have modelled different scenarios. For this, we assumed a DMM source that was contaminated by either upper continental crust (contamination during magma ascent), lower continental crust (contamination, e.g., during residence in a magma chamber reservoir prior to eruption) or a modified, metasomatised source (DMM contaminated with a metasomatic agent). For the two former scenarios, we chose the continental crustal compositions of Rudnick and Gao (2003), for the latter we use global subducting sediment (GLOSS), as proposed by Plank & Langmuir (1998), with low degrees of partial melting for all scenarios ($F \leq 5\%$). It is noted here that the use of a bulk sediment component admixed to a DMM source, e.g., in the course of subduction, is plausible, considering models of sediment mélanges (Marschall and Schumacher 2012).

From the trace element compositions of the erupted lavas, it appears that melting occurred in the spinel rather than the garnet stability field, i.e., at 40 – 80 km depth. Flat HREE patterns are consistent with the presence of spinel and absence of garnet in the mantle source. The lack of a co-variation of $(\text{La}/\text{Sm})_{\text{N}}$ with $(\text{Gd}/\text{Yb})_{\text{N}}$ (where subscript N relates to normalized values to chondritic abundances) further precludes garnet as a residual mineral in the mantle source. Hence, we use partition coefficients (D) that assume a spinel peridotite mantle composition. We add variable amounts of bulk LCC (lower continental crust) and UCC (upper

continental crust, both after Rudnick and Gao 2004), as is the case for crustal contamination, or bulk GLOSS (sediment mélange, Plank and Langmuir 1998) to alter the trace element composition of the source. Subsequently, we assume modal batch melting (Shaw et al., 1970) of this mixed source with variable degrees of melting (F , ranging from 1-5%). Although previous studies noted that source parameters would be variable in relation to changes to the proportions of mineral phases that enter the melt (Guo and Wilson, 2012), we assume that the melting reaction of the source remains unchanged (modal melting); a reasonable assumption for small amounts of crustal addition in a metasomatised source.

As the degree of partial melting and the fraction of the source that has undergone metasomatism are two unknowns, we apply an iterative approach whereby both unknowns have been varied until the compositions of the eruptives have been closely approximated. The resulting model basalt should therefore closely match both the trace element abundances and the radiogenic isotopic compositions of the natural samples. We further note that radiogenic isotope compositions are independent of F , so that the amount of crustal component added is limited by the radiogenic isotope composition of the natural basalts.

The models indicate that a 99:1 to 95:5 mixture of DMM and GLOSS, respectively, can reproduce the unradiogenic isotopic signature of the Tengchong basalts *as well as* their trace element patterns (Figure 9) with a value of 99:1 model giving the best fit (see appendix for further clarification). The degree of melting best representing the trace element patterns and abundances is 1 % in a batch melting scenario. A small degree of olivine fractionation during ascent needs to be acknowledged, as primitive melts would most certainly have higher MgO contents, so the 1 % must be considered as a minimum estimate. Irrespective, variations in the

degree of melting and GLOSS-DMM mixtures are very small with marginal effects on the outcome of the modelling.

All UCC and LCC contamination models fail to reproduce the trace element signatures of the rocks. Because of the higher concentrations of incompatible elements (most importantly Nd+Hf) in partial melts of depleted lithosphere, contamination of a parental basaltic melt requires a much higher degree of assimilation in order to acquire the appropriate isotope composition. For a small degree melt ($F \leq 0.05$), a minimum of 5-10 % of UCC is required to shift the Nd isotope composition from +9 to +1. This change, however, is inconsistent with that permitted in order for the lavas to retain their primitive element chemistry). It is thus concluded that the combined element and isotopic compositions are best explained as being derived from a metasomatised mantle source rather than contamination *en route* to the surface. All other models yield trace element results that are fundamentally different from the abundance patterns observed in the lavas (see appendix for details). In support of this scenario is a comparison of our most primitive samples with primitive continental basalts from the Siberian Traps (Turner and Hawkesworth, 1995), which are considered to be derived from metasomatised lithospheric mantle and indeed display strong similarities in major and trace element characteristics.

The chemical composition and modal mineralogy of shallow sub-continental lithospheric mantle (i.e., within the spinel stability field at ca. 1-2 GPa) is likely to be similar to that of re-fertilised mantle sections in subduction zones where arc lavas are generated. Re-fertilisation is likely to be associated with an injection of Si-C-O-H, along with fluid-mobile elements or bulk sediment melanges. Whilst metasomatised areas may interact with ambient mantle and eventually dissolve into peridotite as pyroxenites, these sections as a whole are expected to

remain relatively stationary in the lithosphere, likely as slivers of hydrated pyroxenites. Such areas are isotopically very different to ambient mantle (Handler et al., 1997; Rudnick et al., 1993; Yaxley et al., 1998), and can reside in the mantle for hundreds of millions if not billions of years (McCoy-West et al., 2013; Wittig et al., 2006). Metasomatism alters parent-daughter ratios of incompatible elements and their radiogenic isotopes bear memory of this parent-daughter fractionation. Following the modelling, it is thus plausible to ascribe the Hf-Nd-Sr-Pb isotope signatures of the most primitive samples to the present day TVF mantle source. Indeed, in terms of Sr-Nd isotopes, our most primitive samples resemble phlogopite-bearing xenoliths from the Australian SCLM (Yaxley et al., 1991, for which no Hf-Pb isotope data is available), adding weight to the interpretation that the radiogenic isotope signatures of the most primitive samples indicate the presence of metasomatised SCLM underneath China.

From the sum of observations, we thus conclude that metasomatised mantle sections preferentially melted in the lithosphere, producing parental liquids identical in radiogenic isotope composition to the two most primitive lavas. From a petrogenetic point of view, this seems plausible, as these sections are likely to melt first upon decompression in the mantle.

5.4 Subduction related metasomatism vs plume origin

An interesting distinction can be made in $^{207}/^{208}\text{Pb}/^{204}\text{Pb}$ vs $^{206}\text{Pb}/^{204}\text{Pb}$ isotope space (Figure 7), in which the most primitive samples plot in a cloud above the NHRL, an area often referred to as so-called Dupal mantle. First described by Dupré and Allègre (1983) and subsequently extended by Hart (1988), Dupal mantle is a consortium of radiogenic isotope signatures deviant from the depleted mantle towards more crustal signatures. In reference to MORB, Dupal mantle is often referred to as Indian mantle, reflecting the offset of Indian MORB

in $^{208}\text{Pb}/^{204}\text{Pb}$ vs $^{206}\text{Pb}/^{204}\text{Pb}$ isotope ratios from Atlantic or Pacific MORB plotting collectively above the NHRL (Figure 7). Because TVF lavas also plot above this line, their genesis has previously been associated with Dupal or Indian mantle (Storey et al., 1989; Tu et al., 1991; Tu et al., 1992; Peate et al., 1999; Meyzen et al., 2005). Whilst MORB-like samples in Eastern China (Zou et al., 2000) plot in the Indian mantle field on Pb isotope diagrams, TVF Pb isotope compositions plot outside the Indian mantle field and require an alternative explanation. Originally, Dupal mantle was related to isotope compositions of oceanic islands deviant from MORB but, these oceanic island signatures are referred to as enriched mantle 1 and 2 (EM1 and EM2, cf. Hoffmann et al., 1997).

Whilst it is argued here that the isotopic compositions of TVF lavas are related to subduction-related metasomatism, for the most primitive samples, there are similarities with EM1/2. In Pb isotope space, a critical test of the resemblance of the TVF lavas with the type locality endmember compositions for EM1 and EM2 is a comparison with eruptives from Pitcairn and Samoa (as type-localities for these endmember compositions), respectively (Figure 10), which shows significant differences. On a $^{208}\text{Pb}/^{204}\text{Pb}$ vs $^{206}\text{Pb}/^{204}\text{Pb}$ diagram, Pitcairn EM1 lava compositions overlap with those of TVF lavas, but this is not observed for $^{207}\text{Pb}/^{204}\text{Pb}$ vs $^{206}\text{Pb}/^{204}\text{Pb}$; EM2 lavas plot away from the TVF samples. Plume-hosted, enriched mantle components represent long-term resident crustal sections, introduced into the mantle via subduction zones and returned to the surface through mantle plumes (e.g., Hofmann et al., 1997). It is plausible that the formation of time-integrated parent daughter ratios through fluid/melt injection into the lithosphere, e.g., in a subduction scenario, create similar isotope signatures. Thus, there is only a partial resemblance between the isotope signatures of intraplate volcanics in SW China and enriched isotope mantle endmembers (namely EM1 or EM2) and a plume origin can be precluded. Notable is that even among mantle plume-derived lavas with an EM1 flavour, isotope differences are expected as to the differences in timescales

of mantle storage of the degree of parent-daughter fractionation in a hypothetical range of EM1 endmembers. However, even considering this diversity, the difference in $^{207}\text{Pb}/^{204}\text{Pb}$ vs $^{206}\text{Pb}/^{204}\text{Pb}$ is too large so that an EM1 resemblance is thoroughly implausible.

Instead, if a metasomatic overprint in the form of sediment mélanges is considered, as indicated by our modelling, an alternative mechanism can be offered that explains the Pb isotope signatures. From the radiogenic isotope compositions, it is clear that the source of the TVF lavas require a time-integrated high κ ($^{232}\text{Th}/^{238}\text{U}$). Slab-derived agents could produce elevated Th concentrations in the mantle. Sediment melt infiltration or the introduction to the TVF mantle source of bulk sediment in the form of a mélange, are plausible explanations for this high κ . Studies of arc-related volcanic rocks indicate that high Th/U is expected in a subduction-related sedimentary component (Turner et al., 1996). Given the extent of the isotopic offset of the TVF data from the NHRL, Th/U fractionation must have either occurred hundreds of millions to more than a billion years ago (for moderate Th/U) or, if this component was introduced more recently, it would have to have had an extremely high Th/U ratio to allow more rapid radiogenic ingrowth. A simple modelling approach indicates that for a $k \sim 10$, ingrowth of 1 Ga is required. Although the exact timing of this event remains elusive, it is clear that the SCLM source of the TVF has a high κ but also low μ (i.e., $^{238}\text{U}/^{204}\text{Pb}$), unlike other metasomatised mantle sources, e.g., in New Zealand (Sprung et al., 2007) or at the Cameroon volcanic line (Rankenburg et al., 2005), indicating that SCLM metasomatism is, as might be expected, chemically diverse.

In summary, it is proposed that the SCLM underneath south-western China is not related to Indian or Dupal mantle, nor is there any evidence for active mantle plume activity; popular plume theories predict an age pattern that is very different to the observed one. Instead, the

enriched mantle signatures of TVF lavas reflect parent-daughter fractionation processes affecting magmas that originated from a metasomatised source with isotopic characteristics similar to those of enriched plume components.

5.5 Tectonic model for the Tengchong volcanics

The melting of SCLM without any notable influence of mantle plume activity raises the question of the cause of partial melting of lithospheric mantle. In addition, and other than is the case for rising plumes, melting below the Tengchong field took place in the spinel stability field, i.e., < 2.5 GPa. It is proposed that the greater plate tectonic regime in the region is responsible for the Cenozoic volcanism in SW China, as was originally proposed by Lightfoot et al., (1993). Rotation of the Indian sub-continent created an extensional tectonic regime that is likely to have caused lithospheric thinning at the junction between the Asian and Indian continental blocks (Figure 11). As for the cause of melting in the absence of active plume involvement, it is suggested that passive upwelling of hot mantle in an extensional setting (Ernst, 2001) is a viable alternative. Melting can simply occur by decompression and does so first in metasomatised mantle sections, which are thus preferentially sampled by intraplate volcanism, or are even their very cause. The solidi of pyroxenitic metasomatised sections are expected to be lower than ambient mantle, which melt preferentially over depleted mantle. It is clear that the Burma-Tengchong terrane underwent west-east extension from ca. 8 Ma (Tapponnier et al., 1982; Harrison et al., 1992; Chen et al., 2002; Socquet and Pubellier, 2005; Mo et al., 2006; Dapeng et al., 2012; Qi et al., 2012; Zhou et al., 2012). It is suggested that this important geodynamic event triggered de-compressional melting of re-fertilised

(metasomatised) mantle in the convergence zone underneath the India-Asia suture, a model also favoured by others for volcanism in southwest China (Lu et al., 2013).

6. Conclusions

On the basis of the combined trace element and Sr-Nd-Pb-Hf isotope compositions of Tengchong volcanic rocks, our conclusions are as follows:

- 1) Cenozoic lavas of the TVF show a broad compositional spectrum in major elements, which, in combination with radiogenic isotopes, indicates an assimilation-fractional crystallization history (AFC). Trends in coupled isotope-element space indicate that all extruding lavas had parental liquids that appear to have been similar in composition.
- 2) Trace element modelling is interpreted to indicate that the mantle source of the TVF lavas was metasomatised sub-continental lithospheric mantle. It is likely that this source was enriched with ca. 1 % of a component similar in composition to bulk subducting sediment and the most primitive lavas were produced by ca. 1% melting of this source material.
- 3) The metasomatised mantle source has time-integrated, high κ ($^{232}\text{Th}/^{238}\text{U}$) and low μ ($^{238}\text{U}/^{204}\text{Pb}$) values, slightly subchondritic $\Sigma_{\text{Nd}}-\Sigma_{\text{Hf}}$ values and moderately radiogenic Sr isotope compositions. These signatures resemble residues of dehydrated sediment, which is likely to have been emplaced during a past subduction event.
- 4) The isotope code of the source is *not* identical to Indian mantle or enriched components in oceanic island lavas.

5) Caution is advised for the use of terms such as EM1, EM2, Indian mantle or Dupal mantle for SCLM, as these terms are generally associated with particular geodynamic processes (e.g., mantle plumes). The source for elevated $^{208}\text{Pb}/^{204}\text{Pb}$ vs $^{206}\text{Pb}/^{204}\text{Pb}$ in SCLM is proposed to be remnants of subducted sediment. Any such component plots (after mantle storage and associated radiogenic ingrowth) above the northern hemisphere reference line. Lithospheric “Dupal mantle” may thus simply be consequent to upper mantle pollution with crustal, sediment-derived components. In analogy, the same may apply to rear- and back-arc portions with so-called Indian-type mantle.

Acknowledgements

J.-W. Park is thanked for assistance with laser ablation analyses of trace elements. O.N. was supported by a Future Fellowship of the Australian Research Council (FT 140101062). T. Cheng was supported by the ANU-China Scholarship Council Program and the National Natural Science Foundation of China (Grant No. 41372072). T. Cheng is particularly grateful to Wei Tian (Peking University) for discussion. The Melbourne T.I.E. team is thanked for constant support. Three anonymous reviewers and Joerg Geldmacher are acknowledged for very insightful reviews and Klaus Mezger for editorial handling, very useful comments and an enormous amount of patience.

References

- Alabaster, T., Pearce, J.A., Malpas, J., 1982. The volcanic stratigraphy and petrogenesis of the Oman ophiolite complex. *Contributions to Mineralogy and Petrology*, 81(3): 168-183.
- Arndt, N., 2013. Intrusions of the Panxi region, China, and their magmatic ore deposits. *Geoscience Frontiers*, 4(5): 479–480
- Aulbach, S., O'Reilly, S., Griffin, W.L., Pearson, N.J., 2008. Subcontinental lithospheric mantle origin of high niobium/tantalum ratios in eclogites, *Nature Geoscience* 1, p. 467-742
- Bédard, J.H., 2006. A catalytic delamination-driven model for coupled genesis of Archaean crust and sub-continental lithospheric mantle. *Geochimica et Cosmochimica Acta*, 70(5): 1188-1214.
- Barling, J., Goldstein, S.L., Nicholls, I.A., 1994. Geochemistry of Heard Island (Southern Indian Ocean):

- characterization of an enriched mantle component and implications for enrichment of the sub-Indian Ocean mantle. *Journal of Petrology*, 35(4): 1017-1053.
- Bouvier, A., Vervoort, J.D., Patchett, P.J., 2008. The Lu-Hf and Sm-Nd isotopic composition of CHUR: constraints from unequilibrated chondrites and implications for the bulk composition of terrestrial planets. *Earth Planetary Science Letters*, 273 (1-2): 48-57
- Brandl, P.A., 2016. Magmatic Evidence for Carbonate Metasomatism in the Lithospheric Mantle underneath the Ohře (Eger) Rift. *Journal of Petrology*, doi: 10.1093/petrology/egv052. First published online: October 13, 2015
- Chen, F., Satir, M., Ji, J., Zhong, D., 2002. Nd-Sr-Pb isotopes of Tengchong Cenozoic volcanic rocks from western Yunnan, China: evidence for an enriched-mantle source. *Journal of Asian Earth Sciences*, 21(1): 39-45.
- Cong, B., Chen, Q., Zhang, R., Wu, G., Xu, P., 1994. The magmatic origin of Tengchong Cenozoic volcanic rocks in western China (in Chinese). *Science in China (Series B)*, 24(4): 441-448.
- Dapeng, L., Zhaohua, L., Jiaqi, L., Yuelong, C., Ye, J., 2012. Magma Origin and Evolution of Tengchong Cenozoic Volcanic Rocks from West Yunnan, China: Evidence from Whole Rock Geochemistry and Nd-Sr-Pb Isotopes. *Acta Geologica Sinica (English Edition)*, 86(4): 867-878.
- Debaille, V., Doucelance, R., Weis, D., Schiano, P., 2006. Multi-stage mixing in subduction zones: Application to Merapi volcano (Java island, Sunda arc). *Geochimica et cosmochimica acta*, 70(3): 723-741.
- Djomani, Y.H.P., O'Reilly, S.Y., Griffin, W., Morgan, P., 2001. The density structure of subcontinental lithosphere through time. *Earth and Planetary Science Letters*, 184(3): 605-621.
- Downes, H., 2001. Formation and modification of the shallow sub-continental lithospheric mantle: a review of geochemical evidence from ultramafic xenolith suites and tectonically emplaced ultramafic massifs of western and central Europe. *Journal of Petrology*, 42(1): 233-250.
- Downes, H., Bodinier, J.-L., Thirlwall, M., Lorand, J.-P., Fabries, J., 1991. REE and Sr-Nd isotopic geochemistry of eastern Pyrenean peridotite massifs: sub-continental lithospheric mantle modified by continental magmatism. *Journal of Petrology*(2): 97-115.
- Dupré, B., Allègre, C.J., 1983. Pb-Sr isotope variation in Indian Ocean basalts and mixing phenomena.
- Eiler, J.M. et al., 1997. Oxygen isotope variations in ocean island basalt phenocrysts. *Geochimica et Cosmochimica Acta*, 61(11): 2281-2293.
- Ernst, R.E., 2001. Contractual effects of mantle plumes on Earth, Mars, and Venus. *Mantle Plumes: Their Identification Through Time*, 352: 103.
- Fan, Q., Liu, R., Wei, H., Shi, L., Sui, J., 1999. The magmatic evolution of the active volcano in the Tengchong area. *Geological Review*, 45(1): 895-904.
- Fan, Q., Sui, J., Liu, R., 2001. Sr-Nd isotopic geochemistry and magmatic evolutions of Wudalianchi Volcano, Tianchi Volcano and Tengchong Volcano. *Acta petrologica et mineralogica*, 20(3): 233-238.
- Griffin, W.L., O'Reilly, S.Y., Abe, N., Aulbach, S., Davies, R.M., Pearson, N.J., Doyle, B.J., Kivi, K., 2003a. The origin and evolution of Archean lithospheric mantle. *Precambrian Research*, 127(1): 19-41.
- Griffin, W.L., O'Reilly, S.Y., Natapov, L.M., Ryan, C.G., 2003b. The evolution of lithospheric mantle beneath the Kalahari Craton and its margins. *Lithos*, 71: 215-241
- Griffin, W., O'Reilly, S.Y., Afonso, J.C., Begg, G., 2009. The composition and evolution of lithospheric mantle: a re-evaluation and its tectonic implications. *Journal of Petrology*, 50(7): 1185-1204.
- Guo, Z., Cheng, Z., Zhang, M., Zhang, L., Li, X., Liu, J., 2015. Post-collisional high-K calc-alkaline volcanism in Tengchong volcanic field, SE Tibet: constraints on Indian eastward subduction and slab detachment. *Journal of the Geological Society*: 2014-078.
- Guo, Z., Wilson, M., 2012. The Himalayan leucogranites: constraints on the nature of their crustal source region and geodynamic setting. *Gondwana Research*, 22(2): 360-376.

- Handler, M.R., Bennett, V.C., Esat, T.M., 1997. The persistence of off-cratonic lithospheric mantle: Os isotopic systematics of variably metasomatised southeast Australian xenoliths. *Earth and Planetary Science Letters*, 151(1): 61-75.
- Harrison, T.M., Wenji, C., Leloup, P., Ryerson, F., Tapponnier, P., 1992. An early Miocene transition in deformation regime within the Red River fault zone, Yunnan, and its significance for Indo-Asian tectonics. *Journal of Geophysical Research: Solid Earth (1978–2012)*, 97(B5): 7159-7182.
- Hart, S.R., 1984. A large-scale isotope anomaly in the Southern Hemisphere mantle. *Nature*, 309: 753-757.
- Hart, S.R., 1988. Heterogeneous mantle domains: signatures, genesis and mixing chronologies. *Earth and Planetary Science Letters*, 90(3): 273-296.
- Hart, S.R., Hauri, E.H., Oschmann, L.A., Whitehead, J.A., 1993. Mantle plumes and entrainment: isotopic evidence, *Science*, 256: 517-520
- Hawkesworth, C.J., Kempton, P.D., Rogers, N.W., Ellam, R.M., & Van Calsteren, P.W., 1990. Continental mantle lithosphere, and shallow level enrichment processes in the Earth's mantle. *Earth and Planetary Science Letters*, 96(3), 256-268.
- Herdt, J., Peate, D., Hawkesworth, C., 1991. The petrogenesis of Mesozoic Gondwana low-Ti flood basalts. *Earth and Planetary Science Letters*, 105(1): 134-148.
- Hoang, N., Uto, K., 2003. Geochemistry of Cenozoic basalts in the Fukuoka district (northern Kyushu, Japan): implications for asthenosphere and lithospheric mantle interaction. *Chemical Geology*, 198(3): 249-268.
- Hofmann A.W., 1997. Mantle geochemistry: The message from oceanic volcanism. *Nature*, 385: 219-229
- Hofmann, A.W., 2004. Sampling mantle heterogeneity through oceanic basalts: isotopes and trace elements. *Treatise on Geochemistry*, 2: 61-101
- Honda, M., Woodhead, J.D., 2005. A primordial solar-neon enriched component in the source of EM-I-type ocean island basalts from the Pitcairn Seamounts, Polynesia. *Earth and Planetary Science Letters*, 236(3): 597-612.
- Hou, Z and Ma, H and Zaw, K and Zhang, Y and Mingjie, W and Zeng, W and Guitang, P and Renli, T, 2003: The Himalayan Yulong Porphyry Copper Belt: Product of Large-Scale Strike-Slip Faulting in Eastern Tibet. *Economic Geology*, 98 (1). pp. 125-145
- Jackson, M.G., Hart, S.R., Koppers, A.A.P., Staudigel, H., Konter, J., Blusztajn, J., Kurz, M., Russell, J.A., 2007. The return of subducted continental crust in Samoan lavas. *Nature*, 448(7154): 684-687.
- Jackson, M.G., Dasgupta, R., 2008. Compositions of HIMU, EM1, and EM2 from global trends between radiogenic isotopes and major elements in ocean island basalts. *Earth and Planetary Science Letters*, 276:175-186.
- Jenner, F.E., O'Neill, H.St.C., Arculus, R.J., Mavrogenes, J.A., 2010, The magnetite crisis in the evolution of arc-related magmas and the initial concentration of Au, Ag, and Cu, *Journal of Petrology*, Vol., 51, p2445-2465
- Jenner, F.E., and O'Neill, H.St.C. 2012, Analyses of 60 elements in 616 ocean floor basaltic glasses, *Geochemistry, Geophysics, Geosystems*, doi.org/10.1029/2011GC004009
- Jiang, C., 1998. Distribution characteristics of Tengchong volcano in the Cenozoic era (in Chinese). *Journal of Seismological research*, 21(4): 309-319.
- Jiang, Y.-H., Jiang, S.-Y., Ling, H.-F., Dai, B.-Z., 2006. Low-degree melting of a metasomatized lithospheric mantle for the origin of Cenozoic Yulong monzogranite-porphyry, east Tibet: geochemical and Sr-Nd-Pb-Hf isotopic constraints. *Earth and Planetary Science Letters*, 241(3): 617-633.
- Jochum, K.P., Weis, U., Stoll, B., Kuzmin, D., Yang, Q., Raczek, I., Jacob, D.E., Stracke, A., Birbaum, K., Frick, D.A., Gunther, D., Enzweiler, J., 2011. Determination of reference values for NIST SRM 610-617 glasses following ISO guidelines. *Geostandards and Geoanalytical Research*, 35(4): 397-429.

- Lassiter, J., Hauri, E., 1998. Osmium-isotope variations in Hawaiian lavas: evidence for recycled oceanic lithosphere in the Hawaiian plume. *Earth and Planetary Science Letters*, 164(3): 483-496.
- Le Maitre, R.W., Igneous Rocks. A Classification and Glossary of Terms. Recommendations of the International Union of Geological Sciences Subcommission on the Systematics of Igneous Rocks, 2nd ed. xvi + 236 pp. Cambridge, New York, Melbourne
- Li, D., Li, Q., Chen, W., 2000. Volcanic activities in the Tengchong volcano area since Pliocene (in Chinese). *Acta Petrologica Sinica*, 16(3): 362-370.
- Li, X.a.L., JQ, 2012. A study on the geochemical characteristics and petrogenesis of Holocene volcanic rocks in the Tengchong volcanic eruption field, Yunnan Province, SW China (in Chinese). *Acta Petrologica Sinica*, 28(5): 1507-1516.
- Lightfoot, P.C. Hawkesworth, C.J., Hergt, J., Naldrett, A.J., Gorbachev, N.S., Fedorenko, V.A., Doherty, W., 1993. Remobilisation of the continental lithosphere by a mantle plume: major-, trace-element, and Sr-, Nd-, and Pb-isotope evidence from picritic and tholeiitic lavas of the Noril'sk District, Siberian Trap, Russia. *Contributions to Mineralogy and Petrology*, 114(2): 171-188.
- Liu, S., Hu, R.Z., Gao, S., Feng, C.X., Huang, Z.L., Lai, S.C., Yuan, H.L., Liu, X.M., Coulson, Ian M., Feng, G.Y., Wang, T., Qi, Y.Q., 2009. U-Pb zircon, geochemical and Sr-Nd-Hf isotopic constraints on the age and origin of Early Palaeozoic I-type granite from the Tengchong-Baoshan Block, Western Yunnan Province, SW China. *Journal of Asian Earth Sciences*, 36: 168-182
- Lu, Y.J., Kerrich, R., Campbell McCuaig, T., Li, Z.X., Hart, C.J.R., Cawood, P.A., Hou, Z.Q., Bagas, L., Cliff, J., Belousova, E.A., Tang, S.A. 2013, Geochemical, Sr-Nd-Pb and zircon Hf-O isotope compositions of Eocene- Oligocene Shoshonitic and Potassic adakite like felsic intrusions in Western Yunnan, SW China: Petrogenesis and tectonic implications, *Journal of Petrology* 54, p 1309-1348
- Marschall, H.R., Schumacher, J.C., 2012. Arc magmas sourced from mélange diapirs in subduction zones. *Nature Geoscience*, 5(12): 862-867.
- McCoy-West, A.J., Bennett, V.C., Puchtel, I.S., Walker, R.J., 2013. Extreme persistence of cratonic lithosphere in the southwest Pacific: Paleoproterozoic Os isotopic signatures in Zealandia. *Geology*, 41(2): 231-234.
- McDonough, W.F., Sun, S.S., 1995. The composition of the Earth. *Chemistry Geology*, 120: 223-253
- Melson W. G., O'Hearn T., and Jarosewitch E., 2002. A data brief on the Smithsonian Abyssal Volcanic Glass Data File. *Geochemistry. Geophysics. Geosystems*. 3, 10.1029/2001GC000249
- Meyzen C.M., Ludden, J.N., Humler, E., Luais, B., Toplis, M.J., Mével, C., Storey, M., 2005. New insights into the origin and distribution of the DUPAL isotope anomaly in the Indian Ocean mantle from MORB of the Southwest Indian Ridge. *Geochemistry, Geophysics, Geosystems*, 6: Q11K11
- Mo, X., Zhao, Z., Deng, J., Flower, M., Yu, X., Luo, Z., Li, Y., Zhou, S., Dong, G., Zhu, D., Wang, L., 2006. Petrology and geochemistry of postcollisional volcanic rocks from the Tibetan plateau: implications for lithosphere heterogeneity and collision-induced asthenospheric mantle flow. *Geological Society of America Special Papers*, 409: 507-530.
- Mu, Z., Tong, W., 1987. Times of volcanic activity and origin of magma in Tengchong Geothermal area, west Yunnan Province (in Chinese). *Acta Geophysica Sinica* 30(3): 261-270.
- Mukasa, S., Shervais, J., Wilshire, H.G., Nielson, J., 1991. Intrinsic Nd, Pb, and Sr isotopic heterogeneities exhibited by the Lherz alpine peridotite massif, French Pyrenees. *Journal of Petrology*(2): 117-134.
- Nägler, T.F., Kramers, J., Kamber, B., Frei, R., Prendergast, M., 1997. Growth of subcontinental lithospheric mantle beneath Zimbabwe started at or before 3.8 Ga: Re-Os study on chromites. *Geology*, 25(11): 983-986.
- Nebel, O., Morel, M.L., Vroon, P.Z., 2009. Isotope dilution determinations of Lu, Hf, Zr, Ta and W, and Hf isotope compositions of NIST SRM 610 and 612 glass wafers. *Geostandards and Geoanalytical Research*, 33(4): 487-499.

- Nebel, O., Vroon, P., van Westrenen, W., Iizuka, T., Davies, G., 2011. The effect of sediment recycling in subduction zones on the Hf isotope character of new arc crust, Banda arc, Indonesia. *Earth and Planetary Science Letters*, 303(3): 240-250.
- Nebel, O., Arculus, R.J., Westrenen, W., Woodhead, J.D., Jenner, F.E., Nebel-Jacobsen, Y.J., Wille, M., and Eggins, S.M., 2013. Coupled Hf-Nd-Pb isotope co-variations of HIMU oceanic island basalts from Mangaia, Cook-Austral islands, suggest an Archean source component in the mantle transition zone, *Geochimica et Cosmochimica Acta*, 112: 87-101.
- Nishio, Y., Nakai, S., Kogiso, T., Barsczus, H.G., 2005. Lithium, strontium, and neodymium isotopic compositions of oceanic island basalts in the Polynesian region: constraints on a Polynesian HIMU origin. *Geochemical Journal*, 39:91-103
- O'Reilly, S., Griffin, W., Poudjom Djomani, Y., Morgan, P., 2001. Are lithospheres forever. Tracking changes in subcontinental lithospheric mantle through time: *GSA Today*, 11(4): 4-10.
- O'Hara, M.J., 1977. Geochemical evolution during fractional crystallization of a periodically refilled magma chamber. *Nature*, 266: 503-507
- Pearce, J.A., Kempton, P., Gill, J., 2007. Hf-Nd evidence for the origin and distribution of mantle domains in the SW Pacific. *Earth and Planetary Science Letters*, 260(1): 98-114.
- Pearce, J.A., Parkinson, I.J., 1993. Trace element models for mantle melting: application to volcanic arc petrogenesis. *Geological Society, London, Special Publications*, 76(1): 373-403.
- Peate, D.W., Hawkesworth, C.J., Mantovani, M.S., Rogers, N.W., Turner, S.P., 1999. Petrogenesis and stratigraphy of the high-Ti/U Urubici magma type in the Paraná flood basalt province and implications for the nature of 'Dupal'-type mantle in the South Atlantic region. *Journal of Petrology*, 40: 451-473
- Pfaender, J., Ratschbacher, L., 2008. Origin of mafic melts in the Pamir mountains—Evidence from trace-element and isotopic data of volcanic and plutonic rocks. *Geochimica et Cosmochimica Acta Supplement*, 72: 743.
- Pfaender, J. A., Jung, S., Münker, C., Stracke, A., Mezger, K., 2012. A possible high Nb/Ta reservoir in the continental lithospheric mantle and consequences on the global Nb budget—Evidence from continental basalts from Central Germany. *Geochimica et Cosmochimica Acta* 77, 232-251.
- Pin, C., Gannoun, A., Dupont, A., 2014. Rapid, simultaneous separation of Sr, Pb, and Nd by extraction chromatography prior to isotope ratios determination by TIMS and MC-ICP-MS, *Journal of Analytical Atomic Spectrometry*, 29; DOI: 10.1039/C4JA00169A
- Pirard, C., Hermann, J., 2015. Experimentally determined stability of alkali amphibole in metasomatised dunite at sub-arc pressures. *Contributions to Mineralogy and Petrology*, 169(1): 1-26.
- Plank, T. and Langmuir, C. . 1998. The chemical composition of subducting sediment and its consequences for the crust and mantle, *Chemical Geology* 145, p325-394
- Qi, X., Zeng, L., Zhu, L., Hu, Z., Hou, K., 2012. Zircon U-Pb and Lu-Hf isotopic systematics of the Daping plutonic rocks: Implications for the Neoproterozoic tectonic evolution of the northeastern margin of the Indochina block, Southwest China. *Gondwana Research*, 21(1): 180-193.
- Qu, X.M., Wang, R.J., Xin, H.B., Jiang, J.H., Chen, H. 2012. Age and Petrogenesis of A-type granites in the middle segment of the Bangonhu-Nujiang suture, Tibetan Plateau, *Lithos*, 146, p. 264-275
- Rankenburg, K., Lassiter, J., Brey, G., 2005. The role of continental crust and lithospheric mantle in the genesis of Cameroon volcanic line lavas: constraints from isotopic variations in lavas and megacrysts from the Biu and Jos Plateaux. *Journal of Petrology*, 46(1): 169-190.
- Reisberg, L., Lorand, J.-P., 1995. Longevity of sub-continental mantle lithosphere from osmium isotope systematics in orogenic peridotite massifs. *Nature*, 376: 159-162.
- Ren, J., Wang, X., OuYang, Z., 2005. Mantle-derived CO₂ in Hot Springs of the Rehai Geothermal Field, Tengchong, China. *Acta Geologica Sinica (English Edition)*, 79(3): 426-431.

- Rudnick, R.L., McDonough, W.F., Chappell, B.W., 1993. Carbonatite metasomatism in the northern Tanzanian mantle: petrographic and geochemical characteristics. *Earth and Planetary Science Letters*, 114(4): 463-475.
- Rudnick, R.L., Gao, S., 2003. Composition of the continental crust. *Treatise on geochemistry*, 3: 1-64
- Shaw, C.R., Prasad, R., 1970. Starch gel electrophoresis of enzymes — a complication of recipes. *Biochemical genetics*, 4:297-320
- Sobolev, A.V., Hofmann, A.W., Kuzmin, D.V., Yaxley, G.M., Arbdt, N.T., Chung, S.L. et al., 2007. The amount of recycled crust in sources of mantle-derived melts. *Science*, 316(5823): 412-417.
- Socquet, A., Pubellier, M., 2005. Cenozoic deformation in western Yunnan (China–Myanmar border). *Journal of Asian Earth Sciences*, 24(4): 495-515.
- Spandler, C., Pirard, C., 2013. Element recycling from subducting slabs to arc crust: a review. *Lithos*, 170: 208-223.
- Sprung, P., Schuth, S., Müunker, C., Hoke, L., 2007. Intraplate volcanism in New Zealand: the role of fossil plume material and variable lithospheric properties. *Contributions to Mineralogy and Petrology*, 153(6): 669-687.
- Storey, M., Saunders, A.D., Tarney, J., Gibson, I.L., Norry, M.J., Thirlwall, M.F., Leats, P., Thompson, R.N., Menzies, M.A., 1989. Contamination of the Indian Ocean asthenosphere by the Kerguelen-Heard mantle plume. *Nature*, 338: 574–576
- Sun, S.-S., McDonough, W., 1989. Chemical and isotopic systematics of oceanic basalts: implications for mantle composition and processes. *Geological Society, London, Special Publications*, 42(1): 313-345.
- Tapponnier, P., Peltzer, G., Le Dain, A., Armijo, R., Cobbold, P., 1982. Propagating extrusion tectonics in Asia: new insights from simple experiments with plasticine. *Geology*, 10(12): 611-616.
- Tu K., Flower M.F.J., Carlson R.W., Zhang M., Xie G., 1991. Sr, Nd, and Pb isotopic compositions of Hainan basalts (south China): implications for a subcontinental lithosphere Dupal source. *Geology*, 19: 567–569
- Tu K., Flower M.F.J., Carlson R.W., Xie G.H., Chen C.Y., Zhang M., 1992. Magmatism in the South China Basin: 1. Isotopic and trace element evidence for an endogenous Dupal mantle component. *Chemical Geol.*, 97 (1992), pp. 47-63
- Turner, S., Arnaud, N., Liu, J., Rogers, N., Hawkesworth, C., Harris, N., Kelley, S., van calsteren, P., Deng, W., 1996, Post-collisional, shoshonitic volcanism on the Tibetan plateau: Implications for convective thinning of the lithosphere and the source of ocean island basalts, *Journal of petrology*, Vol. 37, pp. 45-71
- Turner, S., Hawkesworth, C., 1995. The nature of the sub-continental mantle: constraints from the major-element composition of continental flood basalts. *Chemical Geology*, 120(3): 295-314.
- Vervoort, J.D., Blichert-Toft, J., 1999. Evolution of the depleted mantle: Hf isotope evidence from juvenile rocks through time. *Geochimica et Cosmochimica Acta*, 63(3): 533-556.
- Wang, F., Peng, Z., Zhu, R., He, H., Yang, L., 2006. Petrogenesis and magma residence time of lavas from Tengchong volcanic field (China): evidence from U series disequilibria and $^{40}\text{Ar}/^{39}\text{Ar}$ dating. *Geochemistry, Geophysics, Geosystems*, 7(1).
- Wang, Y., Zhang, X., Jiang, C., Wei, H., Wan, J., 2007. Tectonic controls on the late Miocene–Holocene volcanic eruptions of the Tengchong volcanic field along the southeastern margin of the Tibetan plateau. *Journal of Asian Earth Sciences*, 30(2): 375-389.
- Wasch, L.J., Zwan, F.M., Nebel, O., Morel, M.L.A., Hellebrand, E.W.G., Pearson, D.G., Davies, G.R., 2009. An alternative model for silica enrichment in the Kaapvaal subcontinental lithospheric mantle. *Geochimica et Cosmochimica Acta*, 73(22): 6894-6917.

- Windley, B., Maruyama, S., Xiao, W., 2010. Delamination/thinning of sub-continental lithospheric mantle under Eastern China: The role of water and multiple subduction. *American Journal of Science*, 310(10): 1250-1293.
- Witt-Eickschen, G., 2007. Thermal and geochemical evolution of the shallow subcontinental lithospheric mantle beneath the Eifel: Constraints from mantle xenoliths: a review. In: *Mantle Plumes*, 323-337
- Wittig, N., Baker, J.A., Downes, H., 2006. Dating the mantle roots of young continental crust. *Geology*, 34(4): 237-240.
- Wittig, N., D.G. Pearson, D.G., Duggen, S., Baker, J.A., Hoernle, K., 2010. Tracing the metasomatic and magmatic evolution of continental mantle roots with Sr, Nd, Hf and Pb isotopes *Geochimica et Cosmochimica Acta*, 74: 1417-1435
- Workman, R.K., Hart, S.R., 2005. Major and trace element composition of the depleted MORB mantle (DMM). *Earth and Planetary Science Letters*, 231:53-72.
- Xu, Y., Zhong, D., Liu, j., 2012. Constraints of deep structures on the crust-mantle decoupling in the western Yunnan and the magma activity in the Tengchong volcanic area. *Peogress in Geophysics*, 27(3): 846-855.
- Yaxley, G.M., Crawford, A.J., Green, D.H., 1991. Evidence for carbonatite metasomatism in spinel peridotite xenoliths from western Victoria, Australia. *Earth and Planetary Science Letters*, 107(2): 305-317.
- Yaxley, G.M., Green, D.H., Kamenetsky, V., 1998. Carbonatite metasomatism in the southeastern Australian lithosphere. *Journal of Petrology*, 39(11-12): 1917-1930.
- Yin, G., Li, S., 2000. Theromoluminescence age of last volcanic eruption in Tengchong Maanshan of Yunnan Province (in Chinese). *Journal of Seismological research*, 23(4): 388-391.
- Zhao, C., Chen, T., 1992. A discussion on magma-Tectonic type of cenozoic volcanism from Tengchong area (Yunnan Province) - a new type of post-collision arc-volcanism (in Chinese). *Geoscience*, 6(2): 119-129.
- Zhao, S.W., Lai, S.C., Qin, J.F., Zhu, R.Z., 2014. Zircon U-Pb ages, geochemistry and Sr-Nd-Pb-Hf isotopic compositions of the Pinghe pluton, Southwest China: Implications for the evolution of the Early Paleozoic Proto-Tethys in Southeast Asia. *International Geology Review*, 56: 885-904
- Zhao, Y., Fan, Q., 2010. Magma origin and evolution of Maanshan volcano, Dayingshan volcano and Heikongshan volcano in Tengchong area. *Acta Petrologica Sinica*, 26(4): 1133-1140.
- Zhou, M.-F. et al., 2012. Heterogeneous mantle source and magma differentiation of quaternary arc-like volcanic rocks from Tengchong, SE margin of the Tibetan Plateau. *Contributions to Mineralogy and Petrology*, 163(5): 841-860.
- Zhou, Z., Jiang, C., 1998. Geochemical features of Sr, Nd and Pb isotopes of volcanic rocks in cenozoic era in Tengchong, Changbaishan and Wudalianchi, China (in Chinese) *Journal of Seismological Research*, 21(4): 379-387.
- Zhou, Z., Xiang, C., Yang, H., 2000. Geochemistry of the isotopes in the volcanic rocks in Tengchong, China (in Chinese). *Journal of Seismological research*, 23(2): 194-200.
- Zhu, B., Mao, C., Lugmair, G., MacDougall, J., 1983. Isotopic and geochemical evidence for the origin of Plio-Pleistocene volcanic rocks near the Indo-Eurasian collisional margin at Tengchong, China. *Earth and Planetary Science Letters*, 65(2): 263-275.
- Zhu, R.Z., Lai, S.C., Qin, J.F., Zhao, S.W., 2015. Early Cretaceous highly fractionated I-type granites from the northern Tengchong block, western Yunnan, SW China: Petrogenesis and tectonic implications. *Journal of Asian Earth Sciences*, 100, p. 145-163
- Zou, H.B., Zindler, A., Xu, X.S., Qi, Q., 2000. Major, trace element, and Nd, Sr and Pb isotope studies of Cenozoic basalts in SE China: Mantle sources, regional variations and tectonic significance. *Chemical Geology*, 171: 33-47

Figure captions:

Figure 1: Simplified regional geologic map of the greater Tengchong area, showing the Tengchong volcanic field (TVF) and sample locations (modified geological map 1:200000, Geological survey of Yunnan 1982). Acidic rock refers to highly evolved samples of sub-unit 3.

Figure 2 Total alkali vs. silica (TAS) classification after LeMaitre et al. (2002). Literature sources for other TVF samples are Dapeng et al., 2012 and Zhou et al., 2012. The unit classification of the samples, as detailed in the main text, is based on spatial distribution in the Tengchong block.

Figure 3 Major element variation diagrams for Tengchong samples in comparison with global mid ocean ridge basalts (Melson et al., 2002). Lower Ca content compared to MORB caused by lower degrees of melting and different source mineralogy. The effect is reversed for K₂O.

Figure 4 Primitive mantle normalized multi-element plot for Tengchong samples, showing that the most primitive sample still retains a positive Sr anomaly. Chondrite-normalized REE patterns (values after McDonough and Sun 1995), are shown in the inset. Except for those of the three most isotopically primitive samples, the patterns have negative Eu anomalies, indicating fractionation, including plagioclase. Color scheme as in Figure 3 (orange=unit 1, yellow=unit 1 (primitive), blue=unit 2, green= unit 3, black= cumulate)

Figure 5 MgO (wt. %) versus selected trace element concentrations for Tengchong samples showing the effects of crystal fractionation for Nb, a highly incompatible element, and Ni, which is compatible in olivine. The fractionation curve is the medium through global MORB data (after Jenner and O'Neill 2012)

Figure 6: Sr-Nd-Pb-Hf isotope compositions of all Tengchong samples in comparison with global MORB and intraplate lavas from Eastern China (Hou et al. 2000). In the Sr vs Nd diagram, it is apparent that local granitic crust is a viable contamination endmember in the most evolved samples (taken from Liu et al., 2009). In Hf-Nd isotope space the samples plot slightly above the terrestrial array (after Vervoort et al. 1999). Yellow triangles are samples from unit 1 are among the most primitive samples when compared with published data.

Figure 7 $^{208}\text{Pb}/^{204}\text{Pb}$ vs. $^{206}\text{Pb}/^{204}\text{Pb}$ and $^{207}\text{Pb}/^{204}\text{Pb}$ vs. $^{206}\text{Pb}/^{204}\text{Pb}$ for all Tengchong samples (this study and literature values, pink circles) in comparison with Indian MORB mantle (light grey symbols, taken from the PetDB database, www.petdb.org) and Eastern China volcanic rocks (dark grey circles). The Northern Hemisphere Reference Line (NHRL, after Hart et al., 1984), upper continental crust (UCC) and local upper crust (local UC) are shown for comparison. Local upper crust is taken from Qu et al., 2012 and Zhu et al., 2015. Unit 3 lies on a trend towards local upper crust. All Tengchong samples plot away from Indian MORB.

Figure 8 ϵ_{Nd} versus MgO (wt. %) for Tengchong samples. CHUR is the chondritic uniform reservoir (Bouvier et al., 2008) and epsilon values are the deviation from this reservoir times 10,000. The plot shows a classical trend of assimilation accompanied by fractional crystallisation.

Figure 9 Modelling of the Tengchong volcanic field mantle source. This is performed by first modelling a hypothetical mantle source composed of 99% depleted MORB mantle (DMM, after Workman & Hart, 2005), and addition of a 1% bulk global subducting sediment component (GLOSS, after Plank & Langmuir, 1998). 1% melting of this hybrid source (orange dashed line) produces a model melt composition (blue solid line) that best matches the most primitive Tengchong samples (red solid line). An average composition of melts from the Siberian lithosphere at Nadezhadinsky, Siberia (after Turner and Hawkesworth, 1995, green dotted line) is shown for comparison, showing a similar pattern and thus indicating a similar source and/or process during melting.

Figure 10 Lead isotopes for Tengchong volcanic field (TVF) samples (for clarity Unit 3 and the cumulate sample are omitted) compared with data for ocean island basalt type-localities from Pitcairn (EM1) and Samoa (EM2) (taken from the GEORC database, www.georoc.org). The Northern Hemisphere Reference Line (NHRL, after Hart et al., 1984) is shown for comparison. Whilst the TVF data coincide with the EM1 field in $^{208}\text{Pb}/^{204}\text{Pb}$ - $^{206}\text{Pb}/^{204}\text{Pb}$ isotope space, the $^{207}\text{Pb}/^{204}\text{Pb}$ - $^{206}\text{Pb}/^{204}\text{Pb}$ ratios are different.

Fig.11 Geodynamic sketch for the Tengchong volcanics, indicating the rotation of the sub-Indian microcontinent and Asia, which may have caused passive upwelling of metasomatised sub-continental lithospheric mantle (SCLM). Once metasomatised (i.e., more fertile) mantle crossed the solidus, low-degree partial melting initiated the Tengchong volcanism.

Table 1: Whole rock composition as determined by XRF analyses.

Sample	13-	13-	13-	13-	13-	13-	13-	13-	13-	13-	13-	13-	13-	13-	13-	13-	13-	13-	13-
	LX01	LX02	LX03	LX04	LX05	LX06	LX07	LX08	LX09	LX10	LX11	LX12	LX13	LX14	LX15	LX16	LX17	LX18	LX19
SiO₂	76.07	8.74	77.34	69.67	47.62	48.24	50.12	50.91	51.65	45.54	48.77	48.13	52.55	54.49	52.53	60.26	54.31	53.56	47.92
TiO₂	0.49	0.11	0.54	0.42	1.31	1.34	1.28	1.30	1.34	0.39	1.23	1.23	1.49	1.42	1.47	1.02	1.37	1.38	1.31
Al₂O₃	9.84	2.09	9.14	14.76	15.57	15.69	16.83	17.02	17.65	17.32	16.43	16.20	16.71	16.03	16.57	16.29	17.20	16.45	15.81
Fe₂O₃*	3.12	0.72	2.91	3.14	10.04	11.71	8.22	8.53	8.74	11.60	9.61	10.02	9.51	8.75	9.93	5.75	8.33	7.53	9.91
MnO	0.04	0.01	0.06	0.06	0.15	0.18	0.13	0.14	0.14	0.17	0.15	0.15	0.14	0.13	0.15	0.09	0.13	0.10	0.15
MgO	1.37	1.00	1.20	1.21	7.47	6.96	6.34	6.53	6.22	11.78	7.56	8.14	5.32	4.99	6.16	2.53	4.81	3.46	8.00
CaO	0.97	47.18	1.12	2.91	8.63	8.18	6.98	7.49	7.05	11.86	9.12	8.04	7.92	7.18	7.57	4.78	7.06	5.17	8.13
Na₂O	2.30	0.09	2.25	3.31	2.75	3.19	3.83	4.22	3.72	1.14	3.24	3.17	3.77	3.63	3.87	3.60	3.97	4.12	3.39
K₂O	1.76	0.91	1.70	3.89	1.81	1.60	2.50	2.46	2.48	0.15	1.45	1.54	1.98	2.34	2.15	3.99	2.68	3.42	1.63
P₂O₅	0.13	0.03	0.13	0.13	0.37	0.37	0.52	0.51	0.53	0.05	0.37	0.39	0.37	0.32	0.42	0.41	0.45	0.74	0.40
LOI	3.08	38.54	3.19	0.74	2.99	1.96	2.25	0.01	1.01	0.55	1.68	2.09	0.02	0.02	0.45	0.01	2.69	3.06	
Total	99.17	99.42	99.58	100.24	98.71	99.42	99.00	99.10	100.53	100.55	99.61	99.10	99.78	99.30	100.84	99.17	100.30	98.62	99.71
Mg#	49.3	75.5	47.8	46.1	62.3	56.9	63.1	62.9	61.2	69.3	63.6	64.3	55.4	55.9	57.9	49.4	56.2	50.5	64.2

*Fe₂O₃ is reported as total Fe, LOI is the loss on ignition. The Mg# is defined as the molar Mg/(Fe+Mg).

Table 2: Trace element concentrations as determined by ICP-MS

ppm	13LX01	13LX03	13LX04	13LX05	13LX06	13LX07	13LX08	13LX09	13LX10
Sc	9.51	9.84	9.90	25.16	24.86	20.81	21.37	21.80	21.27
V	60.94	58.08	61.60	159.5	158.4	139.8	144.2	146.6	135.8
Cr	61.70	72.83	30.50	201.8	197.6	134.9	143.8	155.8	99.57
Co	8.21	7.98	6.25	37.71	45.10	27.67	29.58	32.23	60.40
Ni	29.77	25.87	14.62	98.83	97.00	91.63	102.2	109.6	80.70
Co	9.07	8.78	13.11	29.63	27.55	31.90	32.79	32.03	40.77
Zn	49.87	39.77	45.10	80.17	74.33	63.87	70.67	70.60	72.03
Ga	10.95	9.89	16.87	14.98	16.27	16.21	16.54	17.32	12.99
Ge	1.48	1.75	1.86	2.00	2.21	2.03	2.02	1.94	1.71
As	4.18	7.09	2.00	1.92	1.70	2.13	2.18	2.17	1.67
Rb	62.36	58.72	252.8	30.75	21.95	45.79	38.24	37.92	2.69
Sr	80.88	80.51	215.1	659.4	615.7	618.9	664.0	675.4	661.8
Y	18.99	22.28	24.66	22.34	21.81	22.65	23.06	23.62	6.75
Zr	233.5	385.7	173.4	146.4	141.2	200.1	199.2	200.9	18.7
Nb	10.01	11.04	16.55	15.47	14.88	26.60	26.92	27.60	0.98
Mo	0.75	0.91	0.98	1.40	1.36	1.33	2.52	1.78	0.54
Cd	0.07	0.10	0.08	0.13	0.05	0.11	0.12	0.08	0.11
In	0.05	0.05	0.07	0.07	0.06	0.07	0.07	0.08	0.05
Sn	3.53	3.75	7.05	3.43	3.15	3.53	3.65	3.66	2.80
Sb	0.81	0.85	0.72	0.55	0.48	0.56	0.76	0.58	0.55
Ba	305.6	287.4	408.6	502.7	473.0	580.1	576.9	606.1	71.2
La	27.59	34.53	52.39	33.05	31.77	37.36	37.38	38.67	5.14
Ce	53.14	65.85	92.71	60.16	58.62	65.55	65.64	68.46	10.69
Pr	5.94	7.39	9.42	6.85	6.66	7.23	7.39	7.70	1.43
Nd	23.13	28.67	32.24	26.90	26.30	28.14	28.78	29.26	6.54
Sm	4.31	5.27	5.60	5.03	5.06	5.26	5.28	5.39	1.61

Table 2 continued

ppm	13LX11	13LX12	13LX13	13LX14	13LX15	13LX16	13LX17	13LX18	13LX19
Sc	26.72	23.61	24.97	22.12	23.30	14.11	21.41	15.24	24.77
V	185.4	147.5	159.3	144.8	133.3	99.3	144.0	103.5	165.2
Cr	187.8	209.8	142.5	137.0	146.7	34.40	59.33	62.37	215.2
Co	35.73	39.11	30.35	27.27	31.35	13.97	25.63	18.37	37.63
Ni	80.40	135.2	56.60	45.40	52.73	29.67	43.37	44.67	117.1
Co	42.07	42.93	22.50	19.92	21.69	20.08	19.55	13.53	35.80
Zn	73.87	74.90	74.10	77.30	87.47	66.27	70.47	66.83	83.23
Ga	16.65	16.05	17.39	17.42	17.89	18.81	17.85	17.63	16.28
Ge	1.93	2.06	1.95	2.15	2.09	2.23	2.19	1.89	2.14
As	1.97	2.11	1.81	2.26	2.05	2.91	1.78	2.20	2.39
Rb	22.55	24.63	49.18	70.56	35.85	121.7	59.80	58.15	33.58
Sr	767.7	688.4	465.8	408.5	434.7	505.8	552.3	536.5	721.7
Y	20.53	21.80	26.70	26.72	29.29	30.78	27.82	33.97	22.94
Zr	128.0	143.1	170.5	184.9	200.2	343.0	239.0	360.7	149.5
Nb	13.88	16.65	18.65	18.29	24.06	29.45	25.18	39.57	16.62
Mo	1.45	1.33	1.91	2.04	1.73	2.99	2.29	2.57	1.38
Cd	0.10	0.10	0.12	0.12	0.13	0.10	0.11	0.09	0.10
In	0.08	0.07	0.07	0.08	0.08	0.07	0.07	0.07	0.07
Sn	3.33	3.58	3.63	4.18	4.01	4.70	3.55	3.56	3.19
Sb	0.64	0.64	0.65	0.71	0.75	0.63	0.62	0.60	0.56
Ba	556.4	418.5	448.9	441.3	413.7	955.1	652.5	771.9	625.6
La	35.76	29.05	33.50	38.94	32.64	86.17	49.55	64.54	40.84
Ce	62.89	51.53	61.52	73.29	60.52	153.1	89.66	117.90	70.84
Pr	6.93	5.92	7.13	8.20	7.03	16.89	10.01	13.24	7.95
Nd	27.57	23.43	28.02	31.18	28.52	61.07	37.36	49.24	29.95
Sm	5.12	4.50	5.73	6.18	6.10	10.21	7.10	8.58	5.50

Eu	1.53	1.45	1.58	1.50	1.71	1.85	1.81	2.02	1.60
Gd	4.33	4.26	5.37	5.66	5.84	7.69	5.84	7.25	4.96
Tb	0.66	0.66	0.83	0.85	0.92	1.05	0.86	1.04	0.73
Dy	3.85	4.12	5.05	5.22	5.60	5.95	5.29	6.12	4.42
Ho	0.80	0.83	1.03	1.00	1.10	1.17	1.06	1.22	0.88
Er	2.24	2.23	2.90	2.74	3.07	3.19	2.92	3.46	2.47
Tm	0.33	0.34	0.41	0.41	0.44	0.44	0.42	0.51	0.37
Yb	1.95	2.07	2.56	2.56	2.66	2.81	2.68	3.44	2.25
Lu	0.30	0.31	0.38	0.38	0.40	0.43	0.36	0.48	0.33
Hf	2.99	3.26	4.24	4.78	4.70	8.43	5.83	8.11	3.67
Ta	0.78	0.96	1.07	1.11	1.30	1.75	1.41	2.12	0.89
W	0.32	0.28	0.67	0.91	0.35	1.65	0.84	0.89	0.26
Tl	0.01	0.02	0.03	0.06	0.02	0.12	0.03	0.10	0.04
Pb	6.81	5.59	7.37	12.67	6.84	24.43	10.24	12.58	7.69
Bi	0.03	0.03	1.12	0.03	0.19	0.06	0.01	0.06	0.02
Th	7.49	5.89	11.86	18.81	9.77	36.92	15.70	13.93	9.67
U	1.20	0.94	1.26	1.77	0.78	3.13	1.59	1.84	1.33

The trace elements were determined by laser ablation ICP-MS at the ANU on the same fusion discs used for XRF analyses (major elements), using Si as an internal standard and NIST 610 as an external calibrant. Note that sample 13LX02 was not analysed (carbonate samples)

Table 3

sample	$^{87}\text{Sr}/^{86}\text{Sr}$	$\pm 2\sigma$	$^{143}\text{Nd}/^{144}\text{Nd}$	$\pm 2\sigma$	$^{176}\text{Hf}/^{177}\text{Hf}$	$\pm 2\sigma$	$^{206}\text{Pb}/^{204}\text{Pb}$	$\pm 2\sigma$	$^{207}\text{Pb}/^{204}\text{Pb}$	$\pm 2\sigma$	$^{208}\text{Pb}/^{204}\text{Pb}$	$\pm 2\sigma$	εNd	εHf
13LX01	0.724770	16	0.511944	7	0.282407	3	18.556	0.004	15.631	0.003	38.882	0.003	-13.5	-12.9
13LX03	0.724022	11	0.511909	12	0.282326	2	18.573	0.007	15.644	0.007	39.176	0.007	-14.2	-15.8
13LX04	0.718229	11	0.512083	9	0.282656	18	19.133	0.003	15.774	0.004	39.638	0.005	-10.8	-4.1
13LX05	0.706927	12	0.512500	8	0.282912	3	18.214	0.008	15.656	0.008	38.998	0.008	-2.7	+5.0
13LX06	0.706907	15	0.512428	9	0.282918	2	18.248	0.004	15.687	0.004	39.098	0.004	-4.1	+5.2
13LX07	0.705851	16	0.512596	5	0.282937	2	18.318	0.003	15.665	0.005	39.012	0.005	-0.8	+5.8
13LX08	0.705797	18	0.512624	10	0.282936	3	18.323	0.004	15.665	0.003	39.008	0.004	-0.3	+5.8
13LX09#	0.705814	15	0.512671	11	0.282932	3	18.310	0.003	15.648	0.004	38.950	0.005	0.6	+5.7
13LX10	0.707613	14	0.512436	14	0.282624	8	19.054	0.009	15.700	0.009	39.063	0.010	-3.9	-5.3
13LX11	0.705740	15	0.512683	10	0.282968	3	18.306	0.004	15.637	0.004	38.958	0.005	0.9	+6.9
13LX12	0.706030	11	0.512670	6	0.282986	3	18.299	0.003	15.641	0.003	38.935	0.003	0.6	+7.6
13LX13	0.706573	17	0.512474	5	0.282825	3	18.215	0.003	15.669	0.003	39.138	0.003	-3.2	+1.2
13LX14	0.706662	11	0.512369	31	0.282799	2	18.150	0.004	15.665	0.004	39.177	0.005	-5.2	+0.9
13LX15	0.705727	11	0.512560	7	0.282920	2	18.293	0.003	15.677	0.004	39.186	0.004	-1.5	+5.2
13LX16	0.708917	18	n.a.	-	0.282586	2	18.070	0.003	15.658	0.003	39.129	0.004	n.a.	-6.6
13LX17	0.707054	16	0.512410	5	0.282764	2	18.144	0.005	15.644	0.005	39.039	0.005	-4.4	-0.3
13LX18	0.707788	12	0.512349	5	0.282741	2	18.253	0.003	15.672	0.003	39.095	0.004	-5.6	-1.1
13LX19	0.707077	15	0.512488	7	0.282839	3	18.273	0.003	15.667	0.003	39.104	0.003	-2.9	+2.4
13LX02*	0.711350	13	0.511957	210	0.282512	5	19.390	0.006	15.853	0.006	39.472	0.005	-20.3	-9.2
BHVO-2	0.703489	14	0.513044	8	0.283109	8	18.513	0.009	15.522	0.009	38.113	0.010	+8.1	+11.5

Errors are 2 sigma in-run precision of each analyses (in the 6th decimal place for Sr, Nd and Hf). Epsilon notations are the deviation times 10,000 from the chondritic uniform reservoir after

Bouvier et al., (2008)

plutonic cumulate rock, * carbonate, n.a. not analysed.

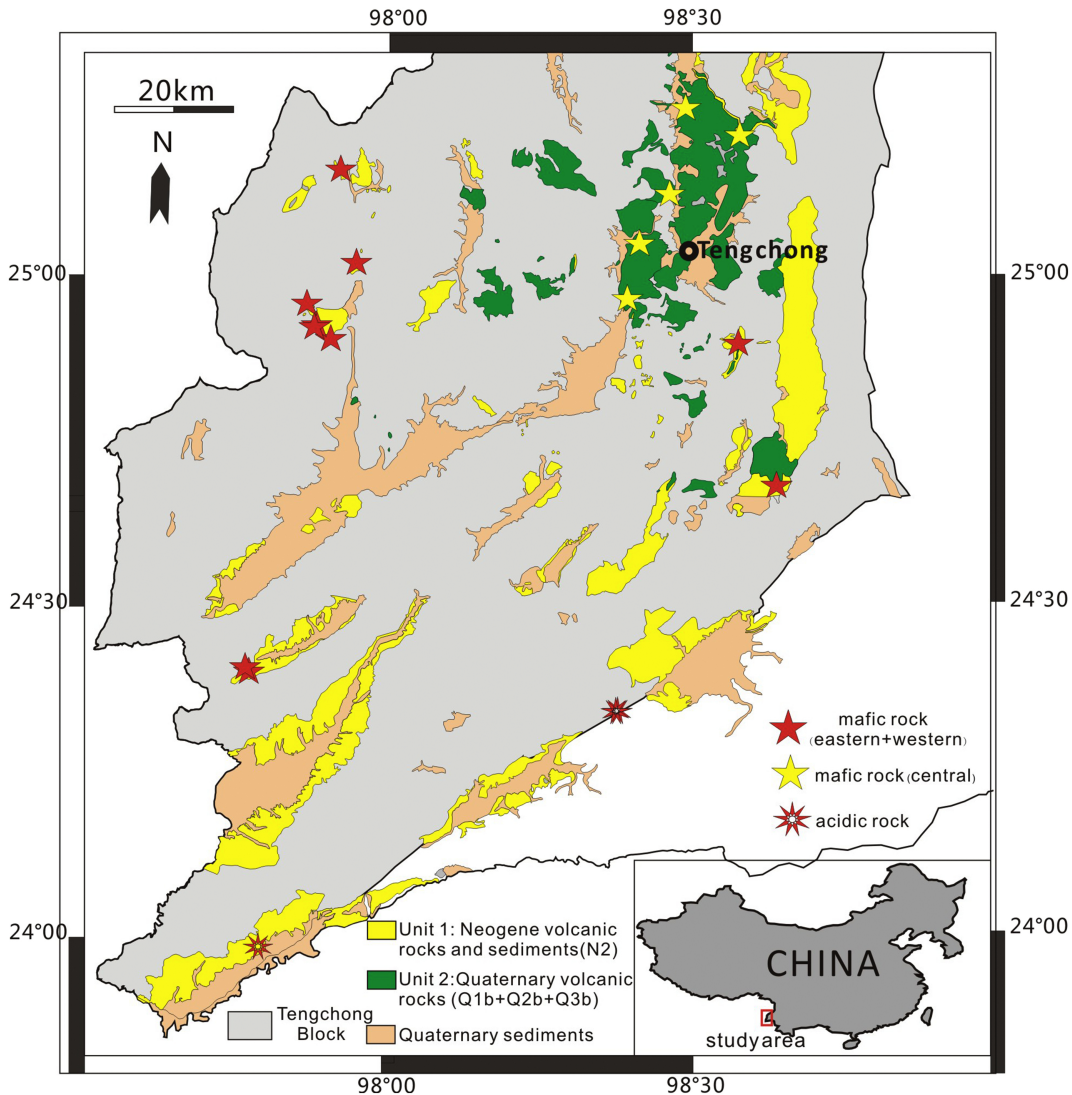


Figure 1

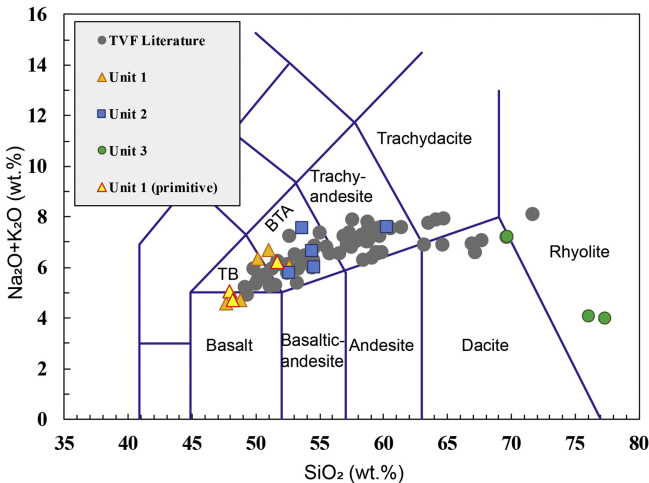


Figure 2

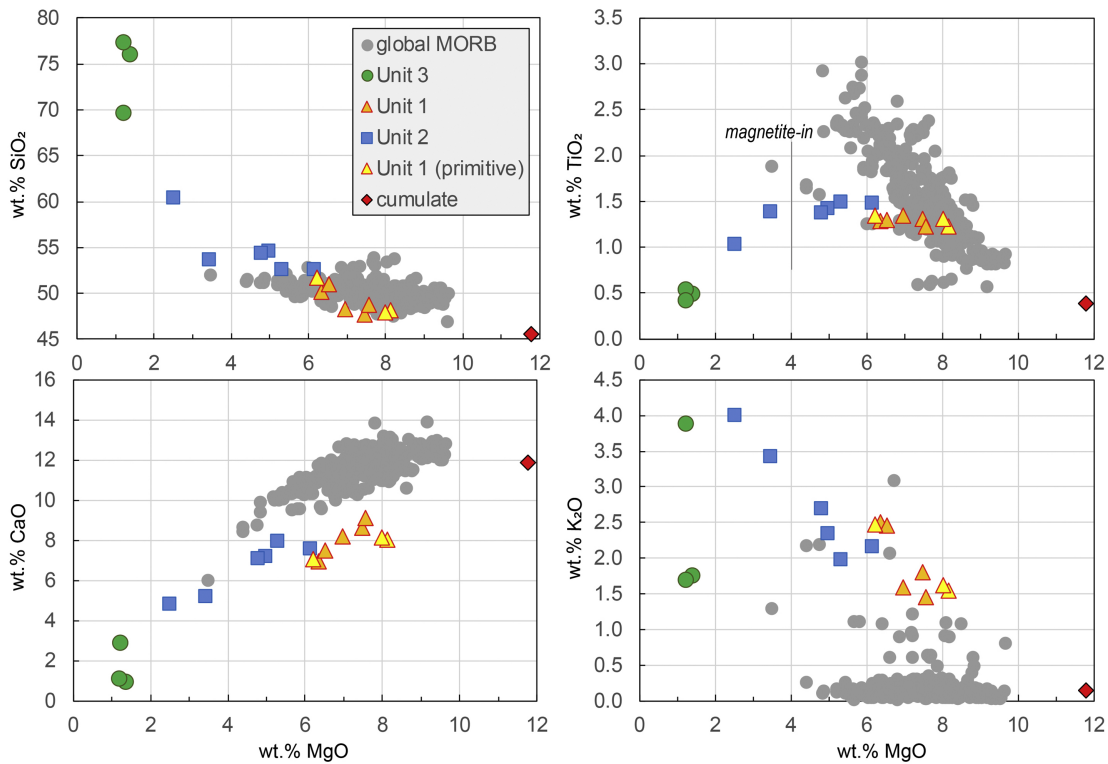


Figure 3

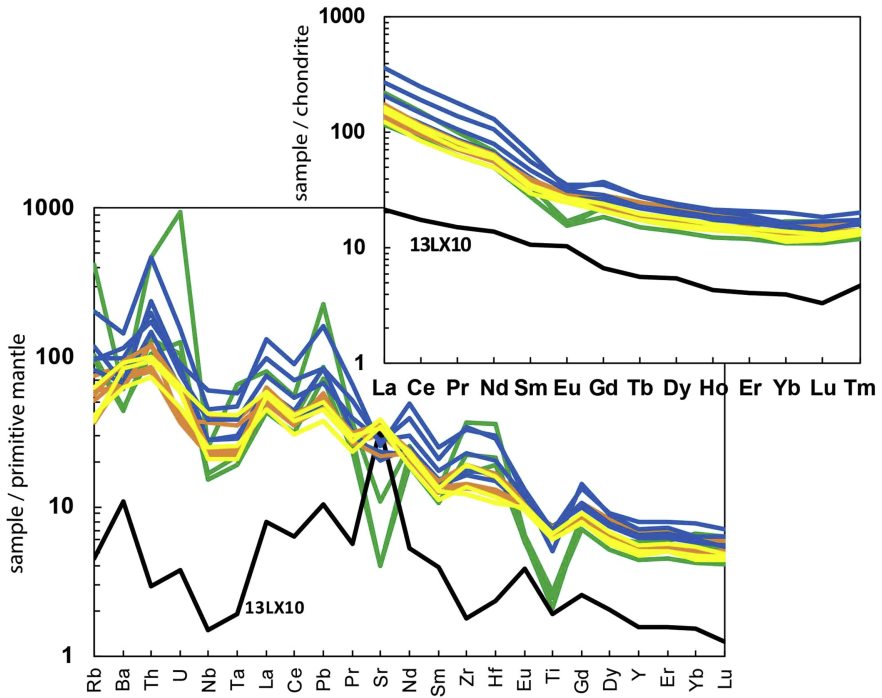


Figure 4

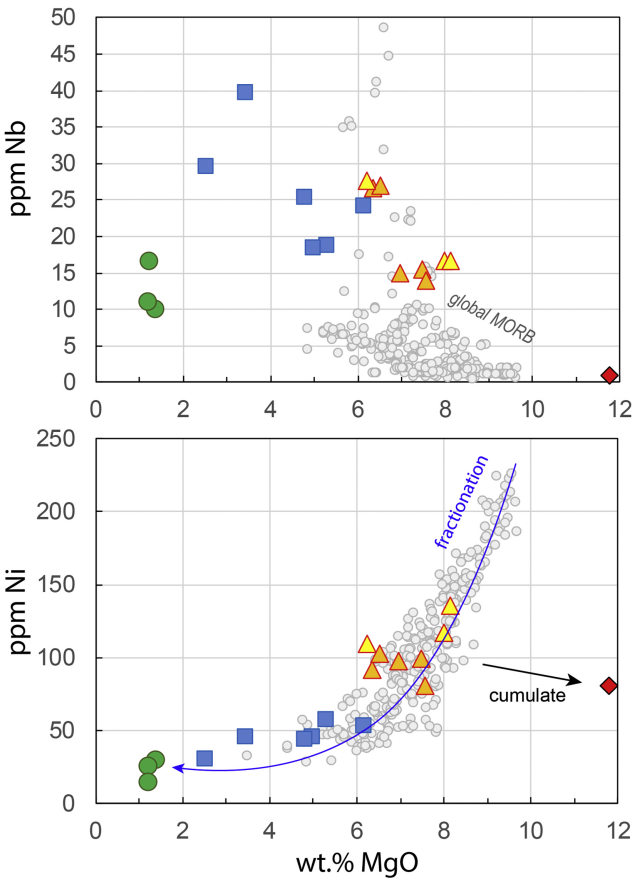


Figure 5

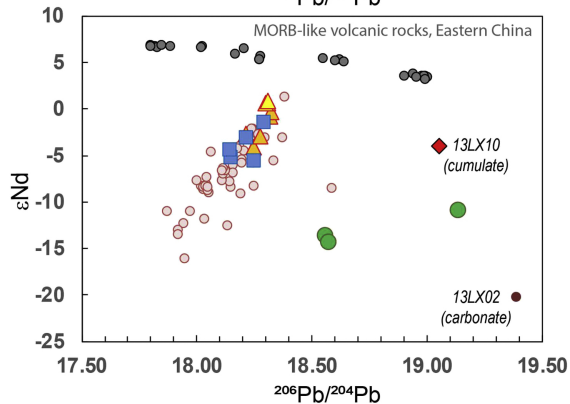
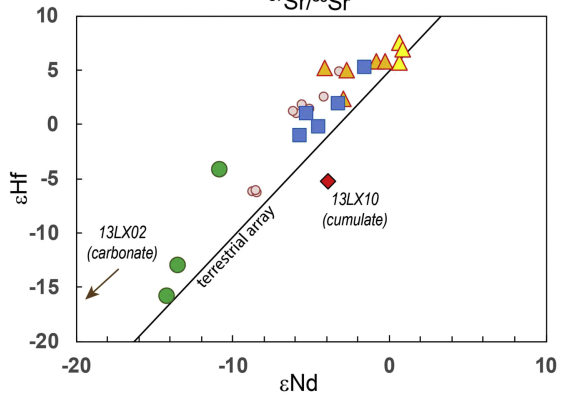
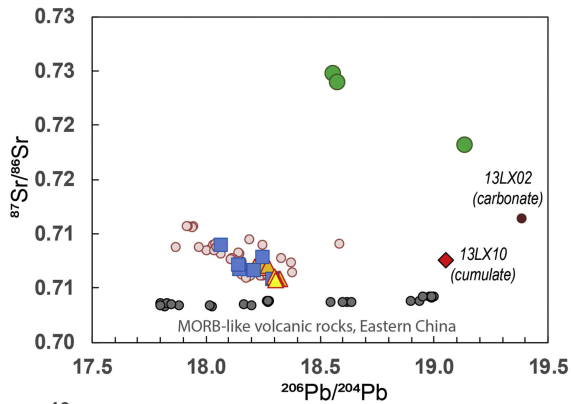
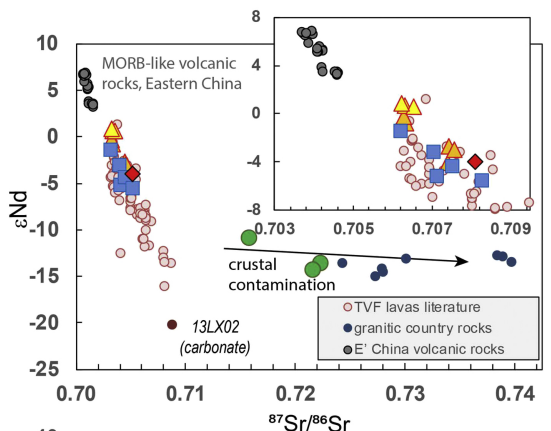


Figure 6

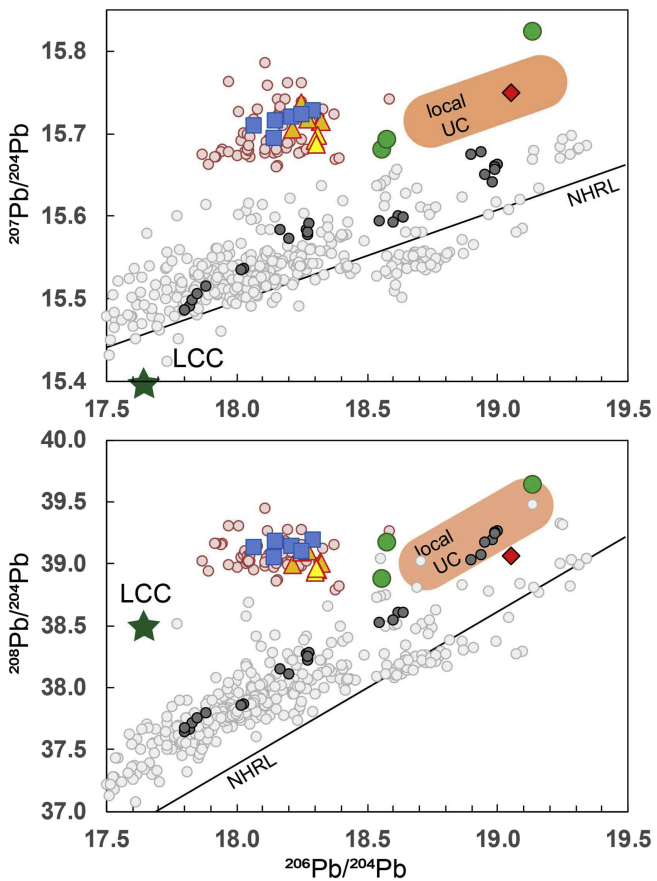


Figure 7

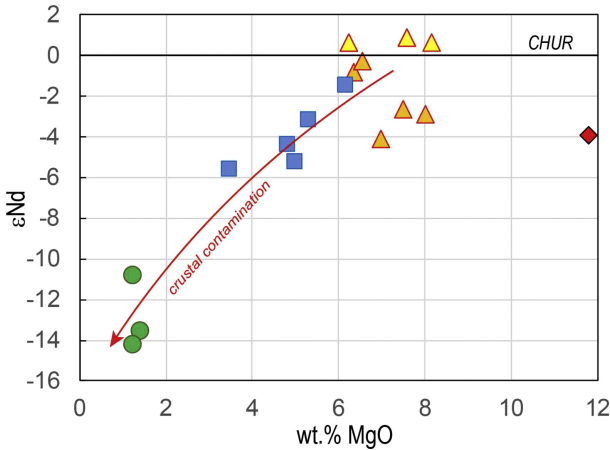


Figure 8

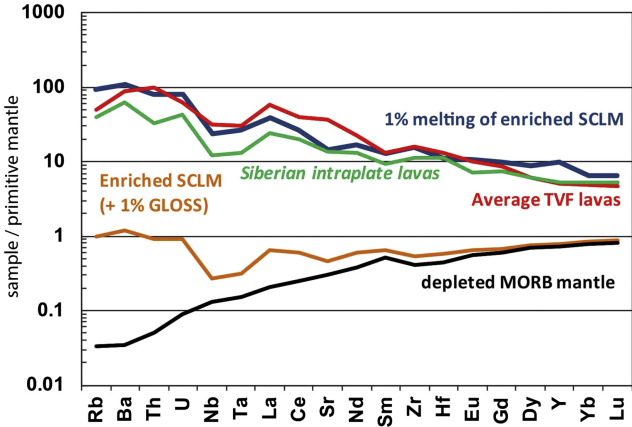


Figure 9

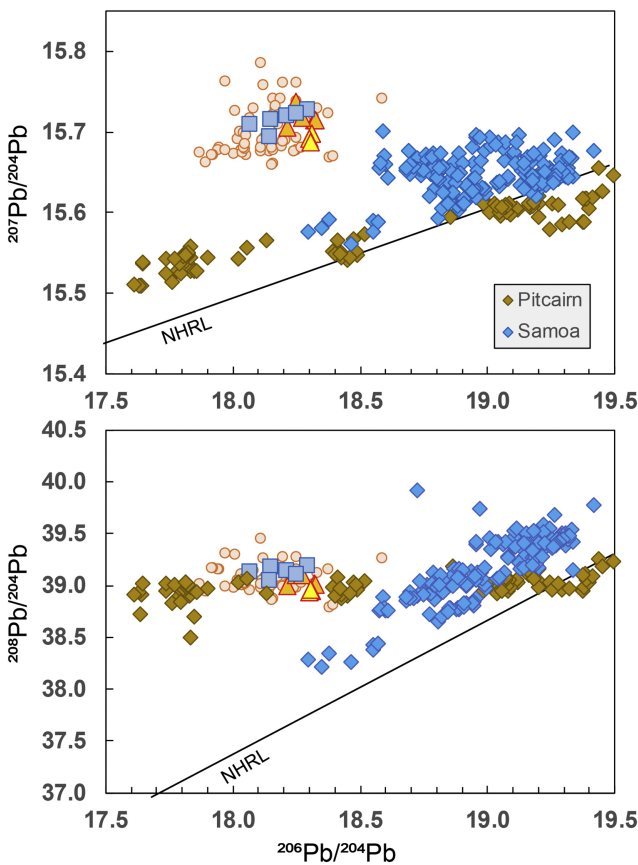


Figure 10

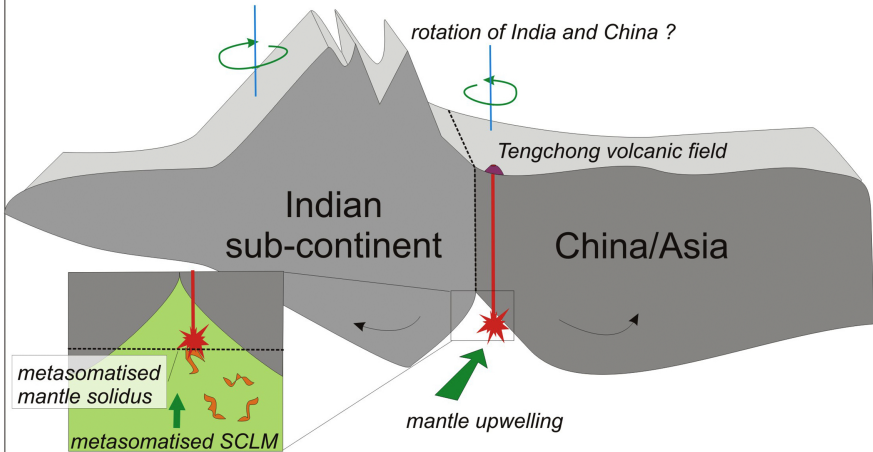


Figure 11